Coordinate regulation of liver ferroportin degradation and *de novo* synthesis determines serum iron levels in mice

Edouard Charlebois[1], Carine Fillebeen[1], Angeliki Katsarou[1], Aleksandr Rabinovich[2#], Kazimierz Wisniewski[2†], Vivek Venkataramani[3,4], Bernhard Michalke[5], Anastasia Velentza[2‡] and Kostas Pantopoulos[1]*

[1] Lady Davis Institute for Medical Research, Jewish General Hospital and Department of Medicine, McGill University, Montreal, Quebec, Canada

[2] Ferring Research Institute Inc, San Diego, CA

[3] Department of Medicine II, Hematology/Oncology, University Hospital Frankfurt, Frankfurt, Germany

[4] Institute of Pathology, University Medical Center Göttingen (UMG), Göttingen, Germany

[5] Helmholtz Zentrum München GmbH – German Research Center for Environmental Health, Research Unit Analytical BioGeoChemistry, Neuherberg, Germany

[#] Current address: 8234 Caminito Maritimo La Jolla CA 92037

[†] Current address: Peptide Logic, LLC, 6185 Cornerstone Ct E, Suite 112, San Diego, CA 92121

[‡] Current address: Plexium, 11494 Sorrento Valley Rd, San Diego, CA 92121

* Corresponding author; tel.: (514) 340-8260 ext. 25293; email: kostas.pantopoulos@mcgill.ca

Abstract

The iron hormone hepcidin is transcriptionally activated by iron or inflammation via distinct, partially overlapping pathways. We addressed how iron affects inflammatory hepcidin levels and the ensuing hypoferremic response. Dietary iron overload did not mitigate hepcidin induction in LPS-treated wt mice but prevented effective inflammatory hypoferremia. Likewise, LPS modestly decreased serum iron in hepcidin-deficient Hjv-/- mice, model of hemochromatosis. Synthetic hepcidin triggered hypoferremia only in control but not iron-loaded wt animals. Furthermore, it dramatically decreased hepatic and splenic ferroportin in Hjv-/- mice on standard or iron-deficient diet, but only triggered hypoferremia in the latter. Mechanistically, iron induced liver ferroportin mRNA translation, thereby antagonizing hepcidin-mediated hypoferremia. Conversely, iron depletion suppressed *de novo* ferroportin synthesis in Hjv-/- livers, allowing exogenous hepcidin to cause hypoferremia. Consequently, prolonged LPS treatment eliminating ferroportin mRNA permitted hepcidin-mediated hypoferremia in iron-loaded mice. Thus, liver ferroportin mRNA translation is critical determinant of serum iron and finetunes hepcidin-dependent functional outcomes. Our data indicate a crosstalk between hepcidin/ferroportin and IRE/IRP systems. Moreover, they suggest that hepcidin supplementation therapy is more efficient combined with iron depletion.

Introduction

Systemic iron balance is controlled by hepcidin a peptide hormone that is produced by hepatocytes in the liver and operates in target cells by binding to the iron exporter ferroportin (1, 2). This results in ferroportin internalization and lysosomal degradation but also directly inhibits ferroportin function by occluding its iron export channel (3, 4). Ferroportin is highly expressed in duodenal enterocytes and tissue macrophages, which are instrumental for dietary iron absorption and iron recycling from senescent erythrocytes, respectively. Ferroportin is also expressed in hepatocytes, where excess iron is stored and can be mobilized on demand. Hepcidin-mediated ferroportin inactivation inhibits iron entry into plasma. This is a critical homeostatic response against iron overload, but also an innate immune response against infection (5). Thus, hepcidin expression is induced when systemic iron levels are high to prevent dietary iron absorption, and also under inflammatory conditions to promote iron retention within ferroportin-expressing cells and render the metal unavailable to extracellular pathogens.

The hepcidin-encoding *HAMP* gene is transcriptionally induced by iron or inflammatory stimuli via BMP/SMAD (6) or JAK/STAT3 (7) signaling, respectively. These pathways crosstalk at different levels. For instance, the BMP co-receptor hemojuvelin (HJV), a potent enhancer of iron-dependent BMP/SMAD signaling, is also essential for inflammatory induction of hepcidin. Thus, Hjv-/- mice, a model of juvenile hemochromatosis characterized by severe iron overload and hepcidin deficiency (8), exhibit blunted inflammatory induction of hepcidin and fail to mount a hypoferremic response following LPS treatment or infection with *E. coli* (9).

Herein, we utilized wild type and Hjv-/- mice to elucidate mechanisms by which systemic iron overload affects downstream hepcidin responses, and particularly, the development of inflammatory hypoferremia.

Results

Dietary iron overload does not prevent further inflammatory Hamp mRNA induction in LPS-treated wt mice, but mitigates hepcidin responsiveness. In an exploratory experiment, wt mice were subjected to dietary iron loading by feeding a high-iron diet (HID) for short (1 day), intermediate (1 week) or long (5 weeks) time intervals; control animals remained on standard diet (SD). As expected, mice on HID for 1 day manifested maximal increases in serum iron (Fig. 1A) and transferrin saturation (Fig. 1B) without changes in total iron-binding capacity (TIBC; Fig. 1C). They retained physiological liver iron content (LIC; Fig. 1E) and serum ferritin (Fig. 1D), a reflection of LIC. Serum iron and transferrin saturation plateaued after longer HID intake, while LIC and serum ferritin gradually increased to peak at 5 weeks. The dietary iron loading promoted gradual upregulation of serum hepcidin and liver *Hamp* mRNA, with highest values at 5 weeks (Fig. 1F-G). This could not prevent chronic dietary iron overload, in agreement with earlier findings (10, 11).

LPS triggered appropriate hepcidin induction and a robust hypoferremic response in control mice. Interestingly, LPS-induced inflammation resulted in further proportional increase in hepcidin and *Hamp* mRNA in dietary iron-loaded mice (Fig. 1F-G). This was accompanied by significant drops in serum iron and transferrin saturation. However, values did not reach the nadir of LPS-treated control animals and were increasing in mice on HID for longer periods,

despite significant hepcidin accumulation. These data suggest that hepatic iron overload does not prevent inflammatory induction of hepcidin; however, it impairs its capacity to mount a hypoferremic response.

Uncoupling inflammatory hepcidin induction from hypoferremic response in dietary iron manipulated wt and Hjv-/- mice. To further explore the potential of hepcidin to promote hypoferremia under iron overload, wt and Hjv-/- mice, a model of hemochromatosis, were subjected to dietary iron manipulations. Wt mice were fed SD or HID, and Hjv-/- mice were fed SD or an iron-deficient diet (IDD) for 5 weeks. Wt mice on HID and Hjv-/- mice on SD or IDD manifested similarly high serum iron and transferrin saturation without changes in TIBC (Fig. 2A-C). Serum non-transferrin bound iron (NTBI) levels were slightly elevated in the dietary and genetic iron overload models and appeared to decrease in Hjv-/- mice on IDD (Fig. 2D). LIC was substantially reduced in Hjv-/- mice in response to IDD, but also compared to wt mice on HID (Fig. 2E). The quantitative LIC data are corroborated histologically by Perls staining (Fig. 2M). Dietary iron loading increased splenic iron in wt mice and confirmed that Hjv-/- mice fail to retain iron in splenic macrophages (Fig. 2N). As expected, hepcidin and *Hamp* mRNA were induced in HID-fed wt mice and were low in Hjv-/- mice on SD, and further suppressed to undetectable levels following IDD intake (Fig. 2F-G).

LPS reduced serum iron and transferrin saturation in hyperferremic wt mice on HID and Hjv-/- mice on SD or IDD, but not below baseline of control wt mice on SD, the only animals that developed a robust hypoferremic response (Fig. 2A-B). The LPS treatment was associated with significant accumulation of hepcidin and induction of *Hamp* mRNA in all experimental groups where this was detectable (Fig. 2F-G), while TIBC, NTBI and LIC were unaffected (Fig. 2C-E). Notably, LPS-treated wt mice on HID and Hjv-/- mice on IDD exhibited dramatic

differences in *Hamp* mRNA but similar blunted hypoferremic response to the acute inflammatory stimulus. Thus, the profound hepcidin induction in iron-loaded wt mice cannot reduce serum iron below that of iron-depleted Hjv-/- mice with negligible hepcidin.

The LPS treatment strongly suppressed liver *Fpn(+IRE)* (ferroportin IRE isoform) mRNA (Fig. 2H) and induced *Dmt1*, *Zip14* and *Lcn2* mRNAs (Figs 2I-K). These encode the divalent metal transporter DMT1, the NTBI transporter Zip14 and the siderophore-binding protein Lcn2, respectively; *Lcn2* mRNA induction was dramatic. The transferrin receptor 1-encoding *Tfrc* mRNA was largely unaffected by LPS, except for a reduction in Hjv-/- mice on IDD (Fig. 2L).

To assess the potential role of hepcidin, we first analyzed ferroportin in the liver, an organ that contributes to iron sequestration during inflammation. Immunohistochemical staining of liver sections revealed strong ferroportin expression in Kupffer cells, predominantly in periportal areas, under all experimental conditions (Figs. 3A and S1). Hepatocellular staining is also evident in the iron overload models, mostly in periportal hepatocytes (Fig. S1), and in line with recent data (12). LPS triggered a shift of ferroportin in Kupffer cells from elongated dendritic branches to round intracellular compartments. LPS did not affect the intensity or distribution of Kupffer cell ferroportin in Hjv-/- mice (Fig. S1), in agreement with previous findings (9).

We further analyzed ferroportin in liver homogenates by Western blotting. Levels of biochemically detectable liver ferroportin differed substantially between wt and Hjv-/- mice. Thus, they were relatively low in the former and highly induced in the latter (Fig. 3B), independently of iron load. The differences were more dramatic compared to those observed by

immunohistochemistry (Figs. 3A and S1). Conceivably, the strong ferroportin signal in Western blots from Hjv-/- liver homogenates reflects high ferroportin expression in hepatocytes, the predominant cell population. Yet, hepatocellular ferroportin is less visible by immunohistochemistry because the signal is substantially weaker compared to that in Kupffer cells. Interestingly, the LPS treatment profoundly suppressed total liver ferroportin in Hjv-/- mice on SD but not IDD, while it modestly affected it in wt mice (Fig. 3B). These data are consistent with negative regulation of ferroportin by residual LPS-induced hepcidin in Hjv-/- mice on SD, which could explain the small drop in serum iron and transferrin saturation under these acute inflammatory conditions, as reported (9). However, liver ferroportin remained detectable and apparently functional, as it did not allow significant iron sequestration and hypoferremia. Notably, a lack of robust hypoferremic response is also evident in LPS-treated wt mice on HID, despite maximal hepcidin and minimal liver ferroportin levels.

Next, we analyzed ferroportin in the spleen, an organ with erythrophagocytic macrophages that plays an important role in body iron traffic. Immunohistochemical analysis shows that LPS reduced ferroportin in red pulp splenic macrophages from wt mice on SD, but this effect was less evident in wt mice on HID and in Hjv-/- mice on SD or IDD (Figs. 3C and S2). Western blot analysis shows a stronger ferroportin signal in splenic extracts from Hjv-/- animals (Fig. 3D), consistent with immunohistochemistry. However, in this assay LPS appeared to suppress splenic ferroportin in all animals except for Hjv-/- mice on IDD. This could be a result of residual hepcidin upregulation (Fig. 2F-G), while the lack of significant splenic ferroportin suppression in Hjv-/- mice on IDD may indicate hepcidin insufficiency. In any case, the lack of hypoferremic response in dietary iron-loaded wt mice indicates continuous iron efflux to plasma despite hepcidin excess.

Is the compromised hypoferremic response to inflammation under iron overload caused by hepcidin insufficiency? We used human synthetic hepcidin to address whether the failure of mouse models of iron overload to mount an appropriate hypoferremic response to acute inflammation is caused by endogenous hepcidin insufficiency or other mechanisms. Wt and Hjv-/- mice subjected to dietary iron manipulations received every two hours 2.5 μg/g synthetic hepcidin for a total of four intraperitoneal injections. Each dose corresponds to ~200-fold excess over endogenous circulating hepcidin in control wt animals. The treatment caused hypoferremia in wt mice on SD but not HID, where the decrease in serum iron was significant but well above baseline of untreated wt controls (Fig. 4A-C). Likewise, synthetic hepcidin significantly decreased serum iron but failed to cause hypoferremia in hepcidin-deficient Hjv-/- mice on SD. Strikingly, hepcidin administration was much more effective in relatively iron-depleted Hjv-/- mice on IDD, and reduced serum iron and transferrin saturation below baseline. The treatments significantly reduced NTBI in Hjv-/- mice on SD, with a trend in mice on IDD (Fig. 4D) but did not affect LIC or splenic iron content (SIC) under any experimental conditions (Figs. 4E-F and S3). Serum iron represents <2% of total tissue iron and therefore its acute fluctuations are not expected to dramatically alter LIC or SIC.

Notably, synthetic hepcidin led to significant reduction of endogenous *Hamp* mRNA in wt mice on SD (Fig. 4G), as earlier reported (13). Conceivably, this is related to destabilization of the Hamp inducer Tfr2 in the liver (Fig. 4H), a known response to hypoferremia (14). Synthetic hepcidin did not promote inflammation, iron perturbations or alterations in BMP/SMAD signaling in the liver, as judged by the unaltered expression of hepatic *Fpn*, *Bmp6* and *Id1* mRNAs (Fig. 4I-K). Moreover, synthetic hepcidin did not affect *Tfrc*, *Dmt1*, *Zip14* or

174 *Lcn2* mRNAs (Fig. S4), which encode iron transporters; *Zip14* and *Lcn2* are also inflammatory
175 markers.

176 Next, we analyzed liver ferroportin by immunohistochemistry. Figs. 5A and S5 show that
177 exogenous hepcidin decreased ferroportin signal intensity in all animal groups to varying
178 degrees. The hepcidin effect was particularly noticeable in hepatocytes from Hjv-/- mice (see
179 low magnification images in Fig. S5). Kupffer cells seemed to retain some ferroportin in all
180 groups except Hjv-/- mice on IDD. Interestingly, while synthetic hepcidin decreased ferroportin
181 signal intensity in Kupffer cells, it did not alter intracellular ferroportin distribution as would be
182 expected based on the data in LPS-treated wt mice (Fig. 5A).

183 Western blotting confirmed that total liver ferroportin is highly induced in Hjv-/- mice
184 (Fig. 5B). Again, the signal intensity can be attributed to protein expressed in hepatocytes. The
185 treatment with synthetic hepcidin did not significantly affect liver ferroportin in wt mice (either
186 on SD or HID), but substantially reduced it in Hjv-/- mice, to almost control levels. The effect
187 appeared more pronounced in Hjv-/- mice on IDD; nevertheless, ferroportin remained detectable.

188 Splenic ferroportin was reduced in all animal groups following hepcidin treatment, with
189 stronger effects visualized by immunohistochemistry in wt mice on SD and Hjv-/- mice on IDD
190 (Figs. 5C and S6). At the biochemical level, ferroportin expression was again much stronger in
191 the spleen of Hjv-/- mice (Fig. 5D). Synthetic hepcidin did not significantly affect splenic
192 ferroportin in wt mice, but dramatically reduced it in all Hjv-/- mice.

193 Taken together, our data suggest that synthetic hepcidin overcomes endogenous hepcidin
194 deficiency in Hjv-/- mice. However, it only triggers hypoferremia in these animals following

relative iron depletion. On the other hand, in iron-loaded wt mice with already high endogenous hepcidin, excess synthetic hepcidin fails to promote hypoferremia.

Iron-dependent regulation of ferroportin mRNA translation in the liver. We hypothesized that the functional outcomes of exogenous hepcidin may not merely depend on its capacity to degrade tissue ferroportin, but also on iron-dependent ferroportin regeneration via *de novo* synthesis. We addressed this in the liver, which can export iron to plasma from ferroportin-expressing parenchymal cells under iron overload. Thus, we assessed the effects of iron on whole liver *Fpn(+IRE)* mRNA translation by polysome profile analysis. Liver extracts from wt mice on SD or HID, and Hjv-/- mice on SD or IDD were fractionated on sucrose gradients to separate translationally inactive light monosomes from translating heavy polysomes. The relative distribution of *Fpn(+IRE)*, *Fth1* (positive control for iron regulation) and Actb (negative control) mRNAs within the different fractions was quantified by qPCR. Fig. 6A shows that dietary iron loading stimulates *Fpn(+IRE)* (and *Fth1*) mRNA translation in wt mice (note the shifts from monosomes to polysomes). Conversely, dietary iron depletion inhibits *Fpn(+IRE)* (and *Fth1*) mRNA translation in Hjv-/- mice. We also attempted to obtain polysome profiles of *Fpn(-IRE)* mRNA but it was undetectable after fractionation. These data indicate that in mouse models of iron overload, iron-stimulated ferroportin synthesis in the liver antagonizes hepcidin-mediated ferroportin degradation and prevents an appropriate hypoferremic response.

Quantification of liver iron by ICP-MS (Fig. 6B) validated iron loading of wt mice by HID, and relative iron depletion of Hjv-/- mice by IDD intake, respectively (see also Fig. 2E). Livers of wt mice on HID had significantly ($p<0.01$) higher iron content compared to Hjv-/- mice on IDD. Iron redox speciation analysis by CE-ICP-MS revealed a profound increase in Fe^{2+}/Fe^{3+} ratios in livers of Hjv-/- mice on SD, which was corrected by dietary iron depletion (Fig. 6C).

Nevertheless, there was no difference in Fe^{2+}/Fe^{3+} ratios among livers of wt mice on SD or HID, and Hjv-/- mice on IDD. We conclude that an increase in total iron content, rather than excessive accumulation of redox active Fe^{2+} drives *Fpn(+IRE)* (and *Fth1*) mRNA translation in the liver.

Effective hypoferremic response to hepcidin in mouse models of iron overload following prolonged LPS treatment that eliminates ferroportin mRNA. We reasoned that complete inactivation of ferroportin mRNA would restore hepcidin-induced hypoferremia despite iron overload. An 8-hour treatment of mice with LPS suppresses liver *Fpn(+IRE)* mRNA below detection levels (Fig. 7A), as reported (9). The same holds true for the *Fpn(-IRE)* isoform (Fig. 7B), which is 290 times less abundant in control mouse livers compared to *Fpn(+IRE)* (ΔCt=8.18), in agreement with published data (15). We went on to examine the effects of synthetic hepcidin on serum iron under these conditions of maximal *Fpn* mRNA suppression. Importantly, the prolonged LPS treatment decreased serum iron in wt mice on HID below the control baseline (Fig. 7C). Furthermore, when combined with synthetic hepcidin, it promoted an effective hypoferremic response in wt mice on HID and Hjv-/- mice on SD (or IDD) (Figs. 7C-E), and tended to decrease NTBI (Fig. 7F). These data strongly suggest that the expression of actively translating *Fpn* mRNA in iron-exporting tissues under systemic iron overload mitigates hepcidin-induced drop in serum iron.

Discussion

We sought to analyze how iron overload affects hepcidin-mediated inflammatory responses. We reported that excess iron inhibits the major hepcidin signaling pathways (BMP/SMAD and IL-6/STAT3) in cultured cells (16). To explore the physiological relevance of

these findings, wt mice were subjected to variable degrees of dietary iron loading and then treated with LPS. All iron-loaded mice could further upregulate hepcidin in response to LPS-induced acute inflammation (Fig. 1). This is consistent with other relevant findings (17) and apparently contradicts the *in vitro* data. While experimental iron loading of cultured cells is rapid, dietary iron loading of mice is gradual (11) and most of excess iron is effectively detoxified within ferritin, which is highly induced (18). By contrast, the suppression of hepcidin preceded ferritin induction in cultured cells (16), which may explain the discrepancy with the *in vivo* data.

We noted that the unimpaired inflammatory induction of hepcidin in iron-loaded wt mice correlated with significant drops in serum iron, but these appeared inversely proportional to the degree of systemic iron loading (Fig. 1). Thus, LPS-treated mice on 5 weeks HID failed to reduce serum iron below a baseline of untreated control mice on SD. This indicates a defect in mounting a hypoferremic response to inflammation, which can be attributed to mechanisms antagonizing hepcidin action. To explore how iron modulates the capacity of hepcidin to trigger inflammatory hypoferremia, we established conditions of iron overload using wt and Hjv-/- mice with extreme differences in hepcidin expression. Figs. 2 and 3 demonstrate that iron overload prevents effective inflammatory hypoferremia independently of hepcidin and tissue ferroportin levels.

We used a ~200-fold excess of synthetic hepcidin to directly assess its capacity to divert iron traffic in iron-loaded mice. Hepcidin injection caused hypoferremia in control wt mice on SD and significantly reduced serum iron in wt mice on HID and Hjv-/- mice on SD, but not below baseline (Fig. 4). Thus, synthetic hepcidin failed to cause hypoferremia in iron overload models with either high or low endogenous hepcidin. Importantly, synthetic hepcidin promoted

robust hypoferremia in relatively iron-depleted Hjv-/- mice on IDD, with undetectable endogenous hepcidin. It should be noted that synthetic hepcidin had similar effects on tissue ferroportin among wt or Hjv-/- mice, regardless of iron diet (Fig. 5). It reduced intensity of the ferroportin signal in Kupffer cells and splenic macrophages of wt mice without significantly affecting biochemically detectable total protein levels. In addition, it dramatically reduced total ferroportin in the liver and spleen of Hjv-/- mice. However, in all experimental settings there was residual tissue ferroportin, which appears to be functionally significant.

We reasoned that at steady-state, tissue ferroportin may consist of fractions of newly synthesized protein, and protein that is *en route* to hepcidin-mediated degradation. Conceivably, the former may exhibit more robust iron export activity, at least before its iron channel gets occluded by hepcidin. Increased *de novo* synthesis of active ferroportin could explain why synthetic hepcidin cannot promote hypoferremia in iron overload. In fact, Fig. 6 demonstrates that dietary iron overload augments *Fpn(+IRE)* mRNA translation in the liver of wt mice. Conversely, relative dietary iron depletion inhibits *Fpn(+IRE)* mRNA translation in the liver of Hjv-/- mice, in line with the restoration of hepcidin-mediated hypoferremic response (Fig. 4).

Considering that *Fpn(+IRE)* is the predominant *Fpn* transcript in the liver (15) and harbors an “iron responsive element” (IRE), our data are consistent with translational control of liver ferroportin expression via the IRE/IRP system. This accounts for coordinate post-transcriptional regulation of iron metabolism proteins in cells (19, 20). In a homeostatic response to iron deficiency, “iron regulatory proteins” IRP1 and IRP2 prevent translation of *Fpn(+IRE)* and *Fth1* mRNAs encoding the iron efflux and storage proteins ferroportin and H-ferritin, respectively, by binding to the IRE within their 5’ untranslated region. IRE/IRP interactions do not take place in iron-loaded cells, allowing *Fpn(+IRE)* and *Fth1* mRNA translation. While

translational control of ferritin is well established (19, 20), regulation of ferroportin by the IRE/IRP system has hitherto only been documented in cell models (21, 22) and the mouse duodenum (23), but not directly validated in the mouse liver. Moreover, the physiological relevance of this mechanism remained speculative.

The critical role of *de novo* ferroportin synthesis in fine-tuning hepcidin-dependent functional outcomes is also highlighted in Fig. 7. Thus, synthetic hepcidin was highly effective as promoter of hypoferremia in dietary iron-loaded wt mice when administered together with LPS. LPS is known to suppress *Fpn* mRNA in cell lines (24) and mouse tissues, with a nadir in the liver reached at 8 h (9). The recovery of hepcidin effectiveness in mouse models of iron overload was only possible when *Fpn* mRNA was essentially eliminated. Under these conditions, LPS treatment alone was sufficient to decrease serum iron in dietary iron-loaded wt mice below baseline.

Tissue iron uptake may be another important determinant of the hypoferremic response to inflammation. LPS did not affect *Tfrc* mRNA levels in the liver (Fig. 2L), which argues against increased uptake of transferrin-bound iron via TfR1. On the other hand, LPS induced *Zip14*, *Dmt1* and *Lcn2* mRNAs (Figs 2J-K). Zip14 is the NTBI transporter accounting for hepatocellular iron overload in hemochromatosis (25) and is upregulated by inflammatory cues in hepatocytes (26). DMT1 is dispensable for NTBI uptake by hepatocytes (27), and its inflammatory induction might promote iron acquisition by macrophages (24, 28). Nevertheless, considering that the fraction of NTBI represents <2% of total serum iron even in the iron overload models (Figs. 2A and D), it is implausible that NTBI uptake by Zip14 and/or DMT1 substantially contributes to inflammatory hypoferremia. Lcn2 is an acute phase protein that can sequester intracellular iron bound to catecholate siderophores (29), and is more likely to transport iron to tissues during

infection. In any case, synthetic hepcidin did not affect expression of iron transporters (Fig. S4). This excludes the possibility for a synergistic effect on LPS-induced tissue iron uptake that could promote effective hypoferremia in the iron overload models.

In conclusion, our data reveal a crosstalk between the hepcidin pathway and the IRE/IRP system in the liver for the control of tissue ferroportin and serum iron levels. Furthermore, they suggest that application of hepcidin therapeutics for treatment of iron overload disorders should be combined with iron depletion strategies to mitigate *Fpn* mRNA translation and increase hepcidin efficacy.

Materials and Methods

Animals. Wild type C57BL/6J and isogenic Hjv-/- mice (30) were housed in macrolone cages (up to 5 mice/cage, 12:12 h light-dark cycle: 7 am - 7 pm; 22 ± 1°C, 60 ± 5% humidity). The mice were fed either a standard diet (200 ppm iron), an iron-deficient diet (2-6 ppm iron) or a high-iron diet (2% carbonyl iron) (31). Where indicated, mice were injected intraperitoneally with 1 µg/g LPS (serotype 055:B5; Sigma-Aldrich) or subcutaneously with 2.5 µg/g synthetic hepcidin; control mice were injected with phosphate-buffered saline. At the endpoints, animals were sacrificed by CO_2 inhalation and cervical dislocation. Experimental procedures were approved by the Animal Care Committee of McGill University (protocol 4966).

Serum biochemistry. Blood was collected via cardiac puncture. Serum was prepared by using micro Z-gel tubes with clotting activator (Sarstedt) and was kept frozen at −20°C until analysis. Serum iron, total iron binding capacity (TIBC) and, where indicated serum ferritin,

were determined at the Biochemistry Department of the Montreal Jewish General Hospital using a Roche Hitachi 917 Chemistry Analyzer. Transferrin saturation was calculated from the ratio of serum iron and TIBC. Serum hepcidin was measured by using an ELISA kit (HMC-001; Intrinsic LifeSciences).

Quantification of serum non-transferrin bound iron (NTBI). NTBI was measured by adapting the method developed by Esposito *et al* (32). Briefly, iron samples of known concentration were created by mixing 70 mM nitrilotriacetate (NTA) (pH = 7.0) with 20 mM ferrous ammonium sulfate. Fe^{2+} was allowed to oxidize to Fe^{3+} in ambient air for at least 30 min and then the solution was diluted to 0.2 mM before further serial dilutions to create a ladder. 5 µl of ladder was loaded in a 96-well plate containing 195 µl plasma-like medium with or without 100 µM deferiprone. The composition of the plasma-like medium was: 40 mg/ml bovine serum albumin, 1.2 mM sodium phosphate dibasic, 120 µM sodium citrate, 10 mM sodium bicarbonate in iron-free HEPES-buffered saline (HEPES 20 mM, NaCl 150 mM, treated with Chelex-100 chelating resin [Bio-Rad, Hercules, CA], 0.5 mM NTA, 40 µM ascorbic acid, 50 µM dihydrorhodamine, pH=7.4). 5 µl of sample was loaded in a 96-well plate containing 195 µl of iron-free HEPES-buffered saline with or without 100 µM deferiprone. Microplates were read every 2 minutes at 37°C over 40 min at 485/520 nm (ex/em). Final NTBI was calculated by comparing the oxidation rate of DHR in the presence or absence of the strong chelator deferiprone.

Hepcidin synthesis. Human hepcidin (DTHFPICIFCCGCCHRSKCGMCCKT) was synthesized at Ferring Research Institute, San Diego, CA. The linear peptide was assembled on Rink amide resin using Tribute peptide synthesizer and the peptide was cleaved from the resin with the TFA/TIS/EDT/H_2O 91:3:3:3 (v/v/v/v) cocktail. The solvents were evaporated, and the

crude peptide was precipitated with diethyl ether, reconstituted in 50% aqueous acetonitrile and lyophilized. The lyophilizate was dissolved in 30% aqueous acetonitrile at the concentration of 0.05 mM and the pH of the solution was adjusted to 7.8 with 6 M ammonium hydroxide. Folding was achieved within 4 hours using the cysteine/cystine redox (peptide/Cys/Cys_2 1:6:6 molar ratio). The reaction mixture was acidified to pH 3, loaded onto HPLC prep column and purified in a TFA based gradient. The identity of the peptide was confirmed by mass spectrometry and by coelution with a commercially available sample (Peptide International, #PLP-3771-PI).

Quantitative real-time PCR (qPCR). RNA was extracted from livers by using the RNeasy kit (Qiagen). cDNA was synthesized from 1 µg RNA by using the OneScript® Plus cDNA Synthesis Kit (Applied Biological Materials Inc.). Gene-specific primers pairs (Table 1) were validated by dissociation curve analysis and demonstrated amplification efficiency between 90-110 %. SYBR Green (Bioline) and primers were used to amplify products under following cycling conditions: initial denaturation 95°C 10 min, 40 cycles of 95°C 5 s, 58°C 30 s, 72°C 10 s, and final cycle melt analysis between 58°-95°C. Relative mRNA expression was calculated by the $2^{-\Delta\Delta Ct}$ method (33). Data were normalized to murine ribosomal protein L19 (*Rpl19*). Data are reported as fold increases compared to samples from wild type mice on standard diet (SD).

Polysome fractionation. RNA was freshly prepared from frozen livers. Linear sucrose gradients were prepared the day before the experiment by using 5% (w/v) and 50% (w/v) sucrose solutions with 10x gradient buffer (200 mM HEPES pH=7.6, 1 M KCl, 50 mM $MgCl_2$, 0.1 mg/ml Cycloheximide, 1 tablet cOmplete™, Mini, EDTA-free Protease Inhibitor Cocktail (Roche), 200 U/mL Recombinant RNasin® Ribonuclease Inhibitor (Promega), 2 mM DTT). Linear gradients were prepared in Polyallomer Centrifuge Tubes (Beckman Coulter). Tubes were marked using a gradient cylinder (BioComp), and 5% sucrose solution was added using a syringe

with a layering needle (BioComp) until solution level reached the mark. Then, 50% sucrose solution was layered underneath the 5% solution until the interface between the two solutions reached the mark. Tubes were capped with rate zonal caps (BioComp) and linearized using a Gradient Master 108 (Biocomp). All reagents were nuclease-free and all solutions were kept on ice or at 4℃. Sample preparation was adapted from Liang *et al.* (34). Briefly, livers were flash frozen upon collection. Roughly 30-80 mg of tissue was crushed using a mortar and pestle in the presence of liquid nitrogen to prevent thawing. Tissues were lysed in up to 1 ml of hypotonic lysis buffer (5 mM Tris-Hcl pH=7.5, 1.5 mM KCl, 2.5 mM $MgCl_2$, 2 mM DTT, 1 mg/ml Cycloheximide, 200 U/ml Recombinant RNasin® Ribonuclease Inhibitor (Promega), 1 tablet cOmplete™, Mini, EDTA-free Protease Inhibitor Cocktail (Roche), 0.5% (v/v) Triton X-100, 0.5% (v/v) Sodium Deoxycholate) and homogenized using Dounce homogenizers (60 movements with both loose and tight pestles) on ice. Samples were centrifuged at 4℃, 16,060g for 4 minutes and supernatants were collected. Sample optical density was measured at 260 nM and samples were normalized to either the lowest value or 30 ODs. 450 µl of sucrose gradient was removed from the top and replaced with normalized sample. Tube weights were balanced by weight before centrifugation at 200,000g for 2 h at 4℃ in a SW 41 Ti rotor and a Beckman Optima L-60 Ultracentrifuge. Samples were fractionated using a BR-188 Density Gradient Fractionation System (Brandel). Immediately upon collection, 800 µl of samples were mixed with 1 ml of TRIzol™ and kept on ice before storage at -80℃. Polysomal RNA was processed according to the manufacturer's protocol. mRNA distribution was analyzed as previously described (35).

Western blotting. Livers were washed with ice-cold PBS and dissected into pieces. Aliquots were snap frozen at liquid nitrogen and stored at −80°C. Protein lysates were obtained

as described (12). Lysates containing 40 µg of proteins were analyzed by SDS-PAGE on 9-13% gels and proteins were transferred onto nitrocellulose membranes (BioRad). The blots were blocked in non-fat milk diluted in tris-buffered saline (TBS) containing 0.1% (v/v) Tween-20 (TBS-T), and probed overnight with antibodies against ferroportin (36) (1:1000 diluted monoclonal rat anti-mouse 1C7, kindly provided by Amgen Inc), β-actin (1:2000 diluted; Sigma), or Tfr2 (1:1000 diluted rabbit polyclonal; Alpha Diagnostics). Following a 3x wash with TBS-T, the membranes were incubated with peroxidase-coupled secondary antibodies for 1 h. Immunoreactive bands were detected by enhanced chemiluminescence with the Western Lightning ECL Kit (Perkin Elmer).

Immunohistochemistry. Tissue specimens were fixed in 10% buffered formalin and embedded in paraffin. Samples were cut at 4-µm, placed on SuperFrost/Plus slides (Fisher) and dried overnight at 37°C. The slides were then loaded onto the Discovery XT Autostainer (Ventana Medical System) for automated immunohistochemistry. Slides underwent de-paraffinization and heat-induced epitope retrieval. Immunostaining was performed by using 1:500 diluted rabbit polyclonal antibodies against ferroportin (37) and an appropriate detection kit (Omnimap rabbit polyclonal HRP, #760-4311 and ChromoMap-DAB #760-159; Roche). Negative controls were performed by the omission of the primary antibody. Slides were counterstained with hematoxylin for four minutes, blued with Bluing Reagent for four minutes, removed from the autostainer, washed in warm soapy water, dehydrated through graded alcohols, cleared in xylene, and mounted with Permount (Fisher). Sections were analyzed by conventional light microscopy and quantified by using the Aperio ImageScope software (Leica Biosystems) (9).

Perls Prussian blue staining. To visualize non-heme iron deposits, deparaffinized tissue sections were stained with Perls' Prussian blue using the Accustain Iron Stain kit (Sigma).

Quantification of liver iron content (LIC). Total liver iron was quantified by using the ferrozine assay (11) or inductively coupled plasma mass spectrometry (ICP-MS) (38).

Iron speciation analysis. Iron redox speciation analysis in the liver was performed by capillary electrophoresis (CE) coupled to ICP-MS (CE-ICP-MS). Dynamic reaction cell (DRC) technology (ICP-DRC-MS) with NH_3 as DRC-gas was applied for non-interfered monitoring of the iron isotopes. A "PrinCe 706" CE system (PrinCe Technologies B.V., Emmen, Netherlands) was employed for separation of iron species at +20 kV. Temperature settings for sample/buffer tray and capillary were set to 20°C. An uncoated capillary (100 cm x 50 µm ID; CS-Chromatographie Service GmbH, Langerwehe, Germany) was used for separation and hyphenation to the ICP–DRC-MS. A CE-ICP-MS interface (38, 39) was installed which provided the electrical connection between CE capillary end and outlet electrode. The self-aspiration mode allowed for best flow rate adjustment and avoided suction flow. Electrolytes for sample stacking and electrophoretic separation were 10% HCl = leading electrolyte, 0.05 mM HCl= terminating electrolyte and 50 mM HCl = background electrolyte. The Fe^{2+}/Fe^{3+} ratio was calculated from quantitative determined concentrations of Fe-species.

Statistics. Statistical analysis was performed by using the Prism GraphPad software (version 9.1.0). Lognormally distributed data including qPCR and ELISA results were first log transformed before analysis with ordinary two-way ANOVA (Tukey's multiple comparisons test) for comparisons within same treatment groups (denoted by a or b on figures) or with multiple unpaired t tests using the Holm-Sidak method to compare effects between treatments.

Normally distributed data was analyzed by two-way ANOVA using either Sidak's method for comparisons between treatment groups or Tukey's multiple comparisons test within treatments groups. Probability value $p<0.05$ was considered statistically significant.

Acknowledgments

We thank Dr. Naciba Benlimame and Lilian Canetti for assistance with histology and immunohistochemistry. This work was supported by a grant from the Canadian Institutes of Health Research (CIHR; PJT-159730). EC was funded by a fellowship from the Natural Sciences and Engineering Research Council of Canada (NSERC) and is currently a recipient of a fellowship from the *Fonds de recherche du Québec – Santé* (FRQS). The work of VV and BM was financially supported by the Deutsche Forschungsgemeinschaft (DFG) through the Priority Program "Ferroptosis: from Molecular Basics to Clinical Applications" (SPP 2306).

References

1. Camaschella C, Nai A, Silvestri L. Iron metabolism and iron disorders revisited in the hepcidin era. Haematologica. 2020;105(2):260-72.
2. Katsarou A, Pantopoulos K. Basics and principles of cellular and systemic iron homeostasis. Mol Aspects Med. 2020;75:100866.
3. Aschemeyer S, Qiao B, Stefanova D, Valore EV, Sek AC, Ruwe TA, et al. Structure-function analysis of ferroportin defines the binding site and an alternative mechanism of action of hepcidin. Blood. 2018;131(8):899-910.
4. Billesbolle CB, Azumaya CM, Kretsch RC, Powers AS, Gonen S, Schneider S, et al. Structure of hepcidin-bound ferroportin reveals iron homeostatic mechanisms. Nature. 2020;586(7831):807-11.
5. Ganz T, Nemeth E. Iron homeostasis in host defence and inflammation. Nat Rev Immunol. 2015;15(8):500-10.
6. Wang CY, Babitt JL. Liver iron sensing and body iron homeostasis. Blood. 2019;133(1):18-29.

7. Schmidt PJ. Regulation of Iron Metabolism by Hepcidin under Conditions of Inflammation. J Biol Chem. 2015;290(31):18975-83.
8. Huang FW, Pinkus JL, Pinkus GS, Fleming MD, Andrews NC. A mouse model of juvenile hemochromatosis. J Clin Invest. 2005;115(8):2187-91.
9. Fillebeen C, Wilkinson N, Charlebois E, Katsarou A, Wagner J, Pantopoulos K. Hepcidin-mediated hypoferremic response to acute inflammation requires a threshold of Bmp6/Hjv/Smad signaling. Blood. 2018;132(17):1829-41.
10. Corradini E, Meynard D, Wu Q, Chen S, Ventura P, Pietrangelo A, et al. Serum and liver iron differently regulate the bone morphogenetic protein 6 (BMP6)-SMAD signaling pathway in mice. Hepatology. 2011;54(1):273-84.
11. Daba A, Gkouvatsos K, Sebastiani G, Pantopoulos K. Differences in activation of mouse hepcidin by dietary iron and parenterally administered iron dextran: compartmentalization is critical for iron sensing. J Mol Med (Berl). 2013;91:95-102.
12. Katsarou A, Gkouvatsos K, Fillebeen C, Pantopoulos K. Tissue-specific regulation of ferroportin in wild type and Hjv-/- mice following dietary iron manipulations. Hepatology Communications. 2021:in press.
13. Laftah AH, Ramesh B, Simpson RJ, Solanky N, Bahram S, Schumann K, et al. Effect of hepcidin on intestinal iron absorption in mice. Blood. 2004;103:3940-4.
14. Johnson MB, Enns CA. Diferric transferrin regulates transferrin receptor 2 protein stability. Blood. 2004;104:4287-93.
15. Zhang DL, Hughes RM, Ollivierre-Wilson H, Ghosh MC, Rouault TA. A ferroportin transcript that lacks an iron-responsive element enables duodenal and erythroid precursor cells to evade translational repression. Cell Metab. 2009;9(5):461-73.
16. Charlebois E, Pantopoulos K. Iron overload inhibits BMP/SMAD and IL-6/STAT3 signaling to hepcidin in cultured hepatocytes. PLoS ONE. 2021;16(6):e0253475.
17. Enculescu M, Metzendorf C, Sparla R, Hahnel M, Bode J, Muckenthaler MU, et al. Modelling Systemic Iron Regulation during Dietary Iron Overload and Acute Inflammation: Role of Hepcidin-Independent Mechanisms. PLoS Comput Biol. 2017;13(1):e1005322.
18. Kent P, Wilkinson N, Constante M, Fillebeen C, Gkouvatsos K, Wagner J, et al. Hfe and Hjv exhibit overlapping functions for iron signaling to hepcidin. J Mol Med (Berl). 2015;93(5):489-98.
19. Wang J, Pantopoulos K. Regulation of cellular iron metabolism. Biochem J. 2011;434(3):365-81.
20. Muckenthaler MU, Galy B, Hentze MW. Systemic iron homeostasis and the iron-responsive element/iron-regulatory protein (IRE/IRP) regulatory network. Annu Rev Nutr. 2008;28:197-213.
21. Lymboussaki A, Pignatti E, Montosi G, Garuti C, Haile DJ, Pietrangelo A. The role of the iron responsive element in the control of ferroportin1/IREG1/MTP1 gene expression. J Hepatol. 2003;39:710-5.
22. Nairz M, Ferring-Appel D, Casarrubea D, Sonnweber T, Viatte L, Schroll A, et al. Iron Regulatory Proteins Mediate Host Resistance to Salmonella Infection. Cell Host Microbe. 2015;18(2):254-61.
23. Galy B, Ferring-Appel D, Becker C, Gretz N, Grone HJ, Schumann K, et al. Iron regulatory proteins control a mucosal block to intestinal iron absorption. Cell Rep. 2013;3(3):844-57.
24. Ludwiczek S, Aigner E, Theurl I, Weiss G. Cytokine-mediated regulation of iron transport in human monocytic cells. Blood. 2003;101:4148-54.

25. Jenkitkasemwong S, Wang CY, Coffey R, Zhang W, Chan A, Biel T, et al. SLC39A14 Is Required for the Development of Hepatocellular Iron Overload in Murine Models of Hereditary Hemochromatosis. Cell Metab. 2015;22(1):138-50.
26. Liuzzi JP, Lichten LA, Rivera S, Blanchard RK, Aydemir TB, Knutson MD, et al. Interleukin-6 regulates the zinc transporter Zip14 in liver and contributes to the hypozincemia of the acute-phase response. Proc Natl Acad Sci USA. 2005;102:6843-8.
27. Wang CY, Knutson MD. Hepatocyte divalent metal-ion transporter-1 is dispensable for hepatic iron accumulation and non-transferrin-bound iron uptake in mice. Hepatology. 2013;58(2):788-98.
28. Wardrop SL, Richardson DR. Interferon-gamma and lipopolysaccharide regulate the expression of Nramp2 and increase the uptake of iron from low relative molecular mass complexes by macrophages. Eur J Biochem. 2000;267(22):6586-93.
29. Xiao X, Yeoh BS, Vijay-Kumar M. Lipocalin 2: An Emerging Player in Iron Homeostasis and Inflammation. Annu Rev Nutr. 2017;37:103-30.
30. Gkouvatsos K, Fillebeen C, Daba A, Wagner J, Sebastiani G, Pantopoulos K. Iron-dependent regulation of hepcidin in Hjv-/- mice: evidence that hemojuvelin is dispensable for sensing body iron levels. PLoS ONE. 2014;9(1):e85530.
31. Fillebeen C, Charlebois E, Wagner J, Katsarou A, Mui J, Vali H, et al. Transferrin receptor 1 controls systemic iron homeostasis by fine-tuning hepcidin expression to hepatocellular iron load. Blood. 2019;133(4):344-55.
32. Esposito BP, Breuer W, Sirankapracha P, Pootrakul P, Hershko C, Cabantchik ZI. Labile plasma iron in iron overload: redox activity and susceptibility to chelation. Blood. 2003;102(7):2670-7.
33. Livak KJ, Schmittgen TD. Analysis of Relative Gene Expression Data Using Real-Time Quantitative PCR and the 2−ΔΔCT Method. Methods. 2001;25(4):402-8.
34. Liang S, Bellato HM, Lorent J, Fernanda, Oertlin C, Vincent, et al. Polysome-profiling in small tissue samples. Nucleic Acids Res. 2018;46(1):e3-e.
35. Panda A, Martindale J, Gorospe M. Polysome Fractionation to Analyze mRNA Distribution Profiles. BIO-PROTOCOL. 2017;7(3).
36. Ross SL, Biswas K, Rottman J, Allen JR, Long J, Miranda LP, et al. Identification of Antibody and Small Molecule Antagonists of Ferroportin-Hepcidin Interaction. Front Pharmacol. 2017;8:838.
37. Maffettone C, Chen G, Drozdov I, Ouzounis C, Pantopoulos K. Tumorigenic properties of iron regulatory protein 2 (IRP2) mediated by its specific 73-amino acids insert. PLoS ONE. 2010;5(4):e10163.
38. Michalke B, Willkommen D, Venkataramani V. Iron Redox Speciation Analysis Using Capillary Electrophoresis Coupled to Inductively Coupled Plasma Mass Spectrometry (CE-ICP-MS). Front Chem. 2019;7:136.
39. Michalke B, Willkommen D, Venkataramani V. Setup of Capillary Electrophoresis-Inductively Coupled Plasma Mass Spectrometry (CE-ICP-MS) for Quantification of Iron Redox Species (Fe(II), Fe(III)). J Vis Exp. 2020(159).

Figures legends

Fig. 1. Dietary iron loading does not disrupt inflammatory hepcidin induction in LPS-treated wild type mice but prevents hepcidin-mediated hypoferremia. Nine-week-old male mice (n=12-14 per group) were fed SD or HID for one day, one week, or five weeks prior to sacrifice. Half of the mice were injected intraperitoneally with saline and the other half with 1 µg/g LPS 4 hours before sacrifice. Sera were collected by cardiac puncture and analyzed for: (A) iron, (B) transferrin saturation, (C) TIBC, (D) ferritin, and (F) hepcidin. Livers were dissected and processed for biochemical analysis of: (E) liver iron content (LIC) by the ferrozine assay and (G) *Hamp* mRNA by qPCR. The dotted line in (A) and (B) indicates baseline serum iron and transferrin saturation, respectively, of control mice on SD. Data (A-E) are presented as the mean±SEM, while (F-G) are presented as geometric mean±SD. Statistically significant differences ($p<0.05$) over time compared to values from saline- or LPS-treated control mice are indicated by a or b, respectively.

Fig. 2. Iron overload prevents hypoferremic response to LPS-induced inflammation in dietary iron-manipulated wt and Hjv-/- mice with dramatic differences in hepcidin expression. Four-week-old male wt mice (n=12-14 per group) were placed on HID for five weeks. Conversely, age- and sex-matched isogenic Hjv-/- mice (n=12-14 per group) were placed on IDD for five weeks to prevent excessive iron overload. Controls from both genotypes were kept on SD. Half of the mice were injected with saline and the other half with 1 µg/g LPS; all animals were sacrificed 4 hours later. Sera were collected by cardiac puncture and analyzed for: (A) iron, (B) transferrin saturation, (C) TIBC, (D) NTBI, and (F) hepcidin. Livers were dissected

582 and processed for LIC quantification by the ferrozine assay (E), and for qPCR analysis of *Hamp*
583 (G), *Fpn(+IRE)* (H), *Dmt1* (I), *Zip14* (J), *Lcn2* (K) and *Tfrc* (L) mRNAs. Sections of liver (M)
584 and spleen (N) were analyzed for iron deposits by Perls' staining (magnification: 10x). The
585 dotted line in (A) and (B) indicates baseline serum iron and transferrin saturation, respectively,
586 of control wt mice on SD. Data in (A-F) are presented as the mean±SEM while in (G-L) are
587 presented as geometric mean±SD. Statistically significant differences ($p<0.05$) compared to
588 values from saline- or LPS-treated wt control mice are indicated by a or b, respectively.

589

590 **Fig. 3. Effects of LPS on hepatic and splenic ferroportin of iron-manipulated wt and Hjv-/-**
591 **mice.** Livers and spleens from mice described in Fig. 2 were dissected and processed for
592 immunohistochemical and biochemical analysis of ferroportin. Immunohistochemical staining of
593 ferroportin in liver (A) and spleen (C) sections (magnification for liver is 20x and for spleen 5x).
594 Western blot for ferroportin and β-actin in liver (B) and spleen (D) extracts from four
595 representative mice in each condition. Blots were quantified by densitometry and ferroportin/β-
596 actin ratios are shown on the right. Densitometric data are presented as the mean±SEM.
597 Statistically significant differences ($p<0.05$) compared to values from saline- or LPS-treated wt
598 control mice are indicated by a or b, respectively.

599

600 **Fig. 4. Iron depletion of Hjv-/- mice improves the efficacy of synthetic hepcidin to promote**
601 **hypoferremia.** Four-week-old wt male mice (n=12-14 per group) were placed on HID for five
602 weeks. Conversely, age- and sex-matched isogenic Hjv-/- mice (n=12-14 per group) were placed
603 on IDD for five weeks to prevent excessive iron overload. Controls from both genotypes were

kept on SD. Half of the mice were injected every 2 hours for a total of 4 injections with saline, and the other half with 2.5 µg/g synthetic hepcidin. Sera were collected by cardiac puncture and analyzed for: (A) iron, (B) transferrin saturation, (C) TIBC, and (D) NTBI. Livers and spleens were dissected and processed for analysis of LIC (E) and SIC (F) by the ferrozine assay. Livers were also used for qPCR analysis of *Hamp* (G), *Fpn(+IRE)* (I), *Bmp6* (J) and *Id1* (K) mRNAs. Finally, livers were used for Western blot analysis of Tfrc, Tfr2, and β-actin; a representative image (out of n=3 samples) is shown in (H). The dotted line in (A) and (B) indicates baseline serum iron and transferrin saturation, respectively, of control wt mice on SD. Data in (A-F) are presented as the mean±SEM while data in (G and I-K) are presented as geometric mean±SD. Statistically significant differences ($p<0.05$) compared to values from saline- or LPS-treated wt control mice are indicated by a or b, respectively.

Fig. 5. Effects of synthetic hepcidin on hepatic and splenic ferroportin of iron-manipulated wt and Hjv-/- mice. Livers and spleens from mice described in Fig. 4 were dissected and processed for immunohistochemical and biochemical analysis of ferroportin. Immunohistochemical staining of ferroportin in liver (A) and spleen (C) sections (magnification for liver is 20x and for spleen 10x). Western blot for ferroportin and β-actin in liver (B) and spleen (D) extracts from four representative mice in each condition. Blots were quantified by densitometry and ferroportin/β-actin ratios are shown on the right. Densitometric data are presented as the mean±SEM. Statistically significant differences ($p<0.05$) compared to values from saline- or hepcidin-treated wt control mice are indicated by a or b, respectively.

626 **Fig. 6. Iron regulation of Fpn(+IRE) mRNA translation in the mouse liver.** Four-week-old
627 wt male mice (n=10-14 per group) were placed on HID for five weeks. Conversely, age- and sex-
628 matched isogenic Hjv-/- mice (n=10-14 per group) were placed on IDD for five weeks to prevent
629 excessive iron overload. Controls from both genotypes were kept on SD. At the endpoint, the
630 mice were sacrificed, and livers were used for polysome profile analysis and iron assays. (A)
631 Liver polysome profiles from n=3 mice in each experimental group. Top: Recording of
632 absorbance at 254 nm of representative samples. Fraction numbers and direction of the gradient
633 are indicated. Bottom left: Distribution of *Fpn(+IRE)*, *Fth1* and *Actb* mRNAs among light
634 monosomal and heavy polysomal fractions (separated by dashed line) was analyzed by qPCR.
635 Bottom right: Bar graph comparisons of pooled fractions. Numbers indicate the fold change
636 compared to wt mice on SD. (B and C) Analysis of total iron (B), and redox iron speciation (C)
637 in the liver by CE-ICP-MS. Data are presented as the mean±SEM. Statistical analysis in (A) was
638 performed by two-way ANOVA and in (B, C) by one-way ANOVA or unpaired t-test.
639 Statistically significant differences ($p<0.05$) compared to values from wt control mice on SD are
640 indicated by *.

641

642 **Fig. 7. Elimination of ferroportin mRNA by prolonged LPS treatment potentiates hepcidin-**
643 **induced hypoferremia in mouse models of iron overload.** Four-week-old wt male mice (n=10-
644 14 per group) were placed on HID for five weeks. Conversely, age- and sex-matched isogenic
645 Hjv-/- mice (n=10-14 per group) were placed on IDD for five weeks to prevent excessive iron
646 overload. Controls from both genotypes were kept on SD. (A and B) Half of the mice were
647 injected with saline and the other half with 1 µg/g LPS and sacrificed after 8 h. Livers were
648 dissected and processed for qPCR analysis of *Fpn(+IRE)* (A) and *Fpn(-IRE)* (B) mRNAs. (C-F)

649 All mice were injected with 1 µg/g LPS. Half of the animals were subsequently injected with
650 saline, and the other half with 2.5 µg/g synthetic hepcidin every two hours for a total of 4
651 injections. At the endpoint the mice were sacrificed. Sera were collected by cardiac puncture and
652 analyzed for: (C) iron, (D) transferrin saturation, (E) TIBC, and (F) NTBI. The dotted line in (C)
653 and (D) indicates baseline serum iron and transferrin saturation, respectively, of control wt mice
654 on SD. Data are presented as (A-B) geometric mean±SD or (C-F) mean±SEM. Statistically
655 significant differences ($p<0.05$) compared to values from saline-treated (A and B) or
656 LPS/hepcidin-treated (C and F) wt control mice on SD are indicated by a, b or c, respectively.

657

658

659

660

Table 1. List of primers used for qPCR.

Gene	GenBank accession	Forward primer sequence	Reverse primer sequence
Hamp1	NM_032541.1	*AAGCAGGGCAGACATTGCGAT*	*CAGGATGTGGCTCTAGGCTATGT*
Fpn(+IRE)	NM_016917.2	*GGCATAAGGCTGTTGTGCTT*	*TCATGACACCAGGCGTTCTC*
Fpn(-IRE)	XM_006496137.4	*GCCGGTTGGAGTTTCAATGT*	*TCATGACACCAGGCGTTCTC*
Dmt1	NM_001146161.1	*CTTGGGATACTGACGGTGAC*	*GATTTGCAGTCTGGAGCAGT*
Zip14	NM_001135151.1	*TGGATAGTGAGGCTGCGTGG*	*ATGGTGAGGCCAAGGCTAAT*
Lcn2	NM_008491	*GGCCAGTTCACTCTGGGAAA*	*TGGCGAACTGGTTGTAGTCC*
Tfrc	NM_011638.4	*AGCCAGATCAGCATTCTCTAACT*	*GCCTTCATGTTATTGTCGGCAT*
Bmp6	NM_007556.2	*ACTCGGGATGGACTCCACGTCA*	*CACCATGAAGGGCTGCTTGTCG*
Id1	NM_010495.2	*GGTACTTGGTCTGTCGGAGC*	*GCAGGTCCCTGATGTAGTCG*
Fth1	NM_010239.2	*AAGTGCGCCAGAACTACCAC*	*AGCCACATCATCTCGGTCAA*
Rpl19	NM_009078.2	*AGGCATATGGGCATAGGGAAGAG*	*TTGACCTTCAGGTACAGGCTGTG*
Actb	NM_007393.3	*GACGACATGGAGAAGATCTG*	*GTGAAGCTGTAGCCACGCTC*

661

662

663

Supplemental Figure legends

Fig. S1. Low magnification immunohistochemical images of ferroportin in liver sections of dietary iron-manipulated wild type and Hjv-/- mice following LPS treatment. Liver sections from mice described in Fig. 2 were used for immunohistochemical analysis of ferroportin (magnifications: 10x and 5x).

Fig. S2. Low magnification immunohistochemical images of ferroportin in spleen sections of dietary iron-manipulated wild type and Hjv-/- mice following LPS treatment. Spleen sections from mice described in Fig. 2 were used for immunohistochemical analysis of ferroportin (magnification: 2x).

Fig. S3. Perls staining for iron deposits in liver and spleen sections of dietary iron-manipulated wild type and Hjv-/- mice following treatment with synthetic hepcidin. Liver and spleen sections from mice described in Fig. 4 were stained with Perls Prussian blue (magnification: 10x).

Fig. S4. Effects of LPS treatment on expression of mRNAs encoding iron transport proteins in the liver of dietary iron-manipulated wild type and Hjv-/- mice. Livers from mice described in Fig. 2 were dissected and processed for qPCR analysis of mRNAs encoding iron transport proteins. (A) *Tfrc* mRNA, (B) *Dmt1* mRNA, (C) *Zip14* mRNA and (D) *Lcn2* mRNA. All data are presented as the geometric mean ± SD. Statistically significant differences ($p<0.05$)

compared to values from saline- or LPS-treated control mice are indicated by a or b, respectively.

Fig. S5. Low magnification immunohistochemical images of ferroportin in liver sections of dietary iron-manipulated wild type and Hjv-/- mice following treatment with synthetic hepcidin. Liver sections from mice described in Fig. 4 were used for immunohistochemical analysis of ferroportin (magnifications: 10x and 5x).

Fig. S6. Low magnification immunohistochemical images of ferroportin in spleen sections of dietary iron-manipulated wild type and Hjv-/- mice following treatment with synthetic hepcidin. Spleen sections from mice described in Fig. 4 were used for immunohistochemical analysis of ferroportin (magnification: 2x).

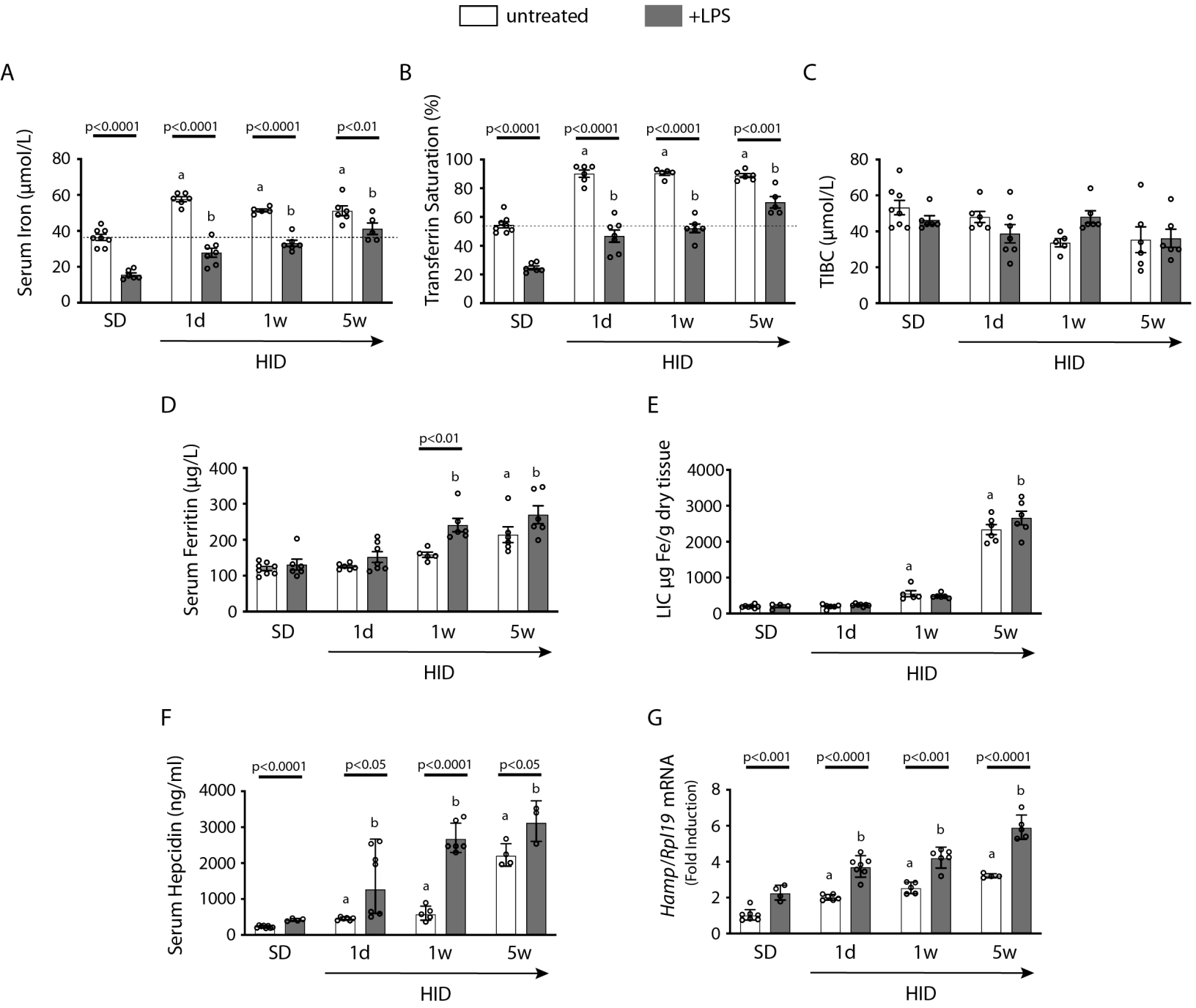

Fig. 1

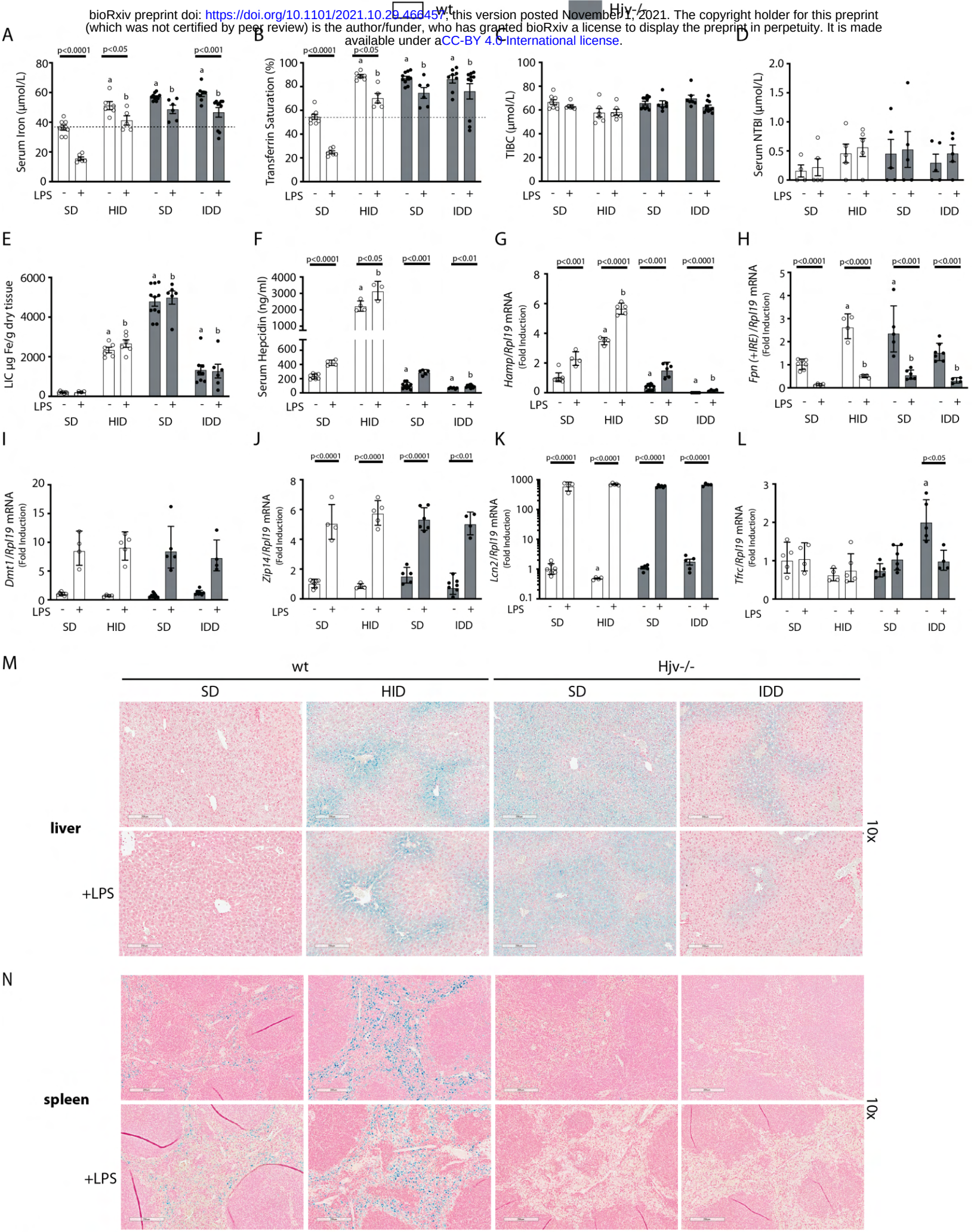

Fig. 2

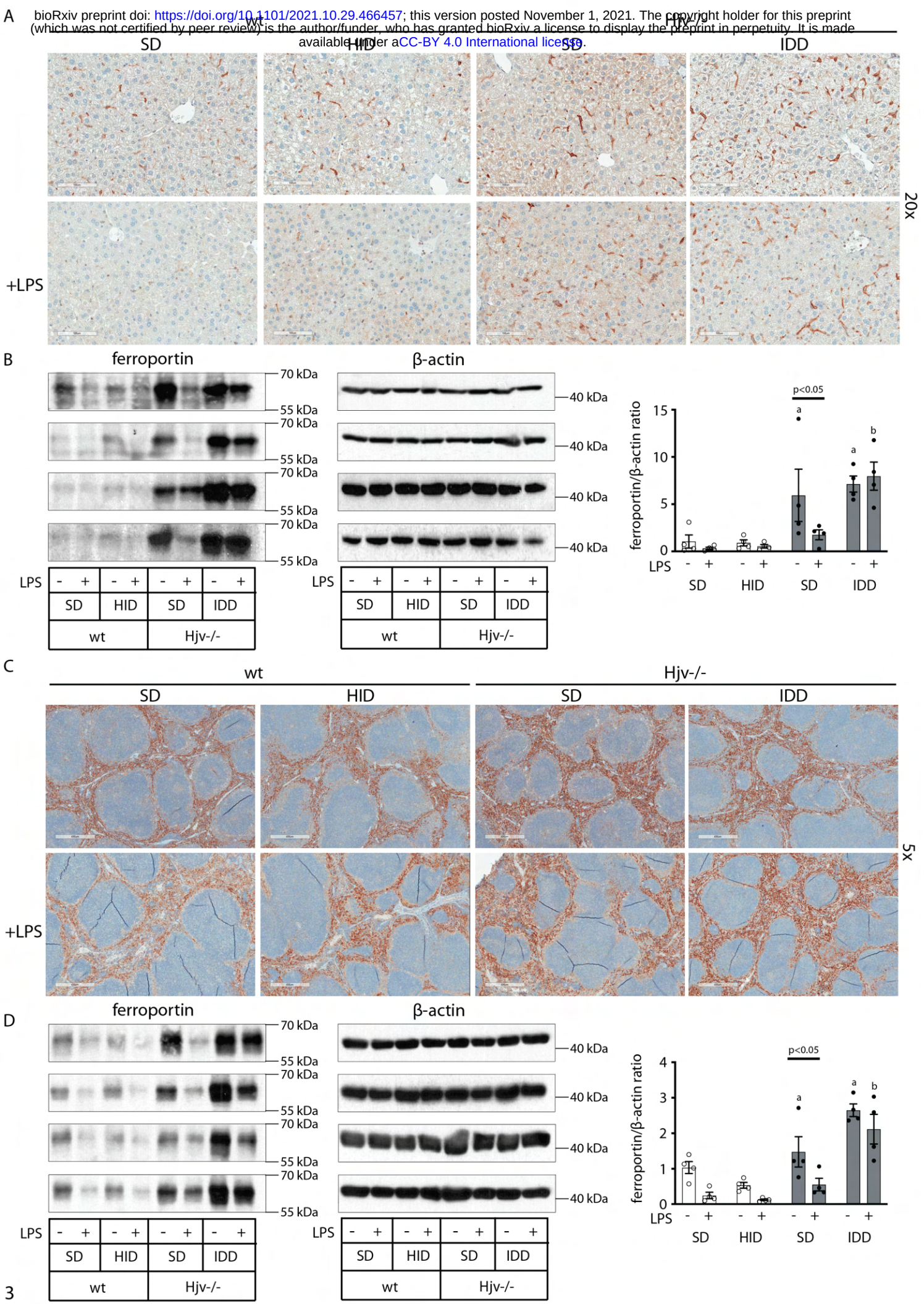

Fig. 3

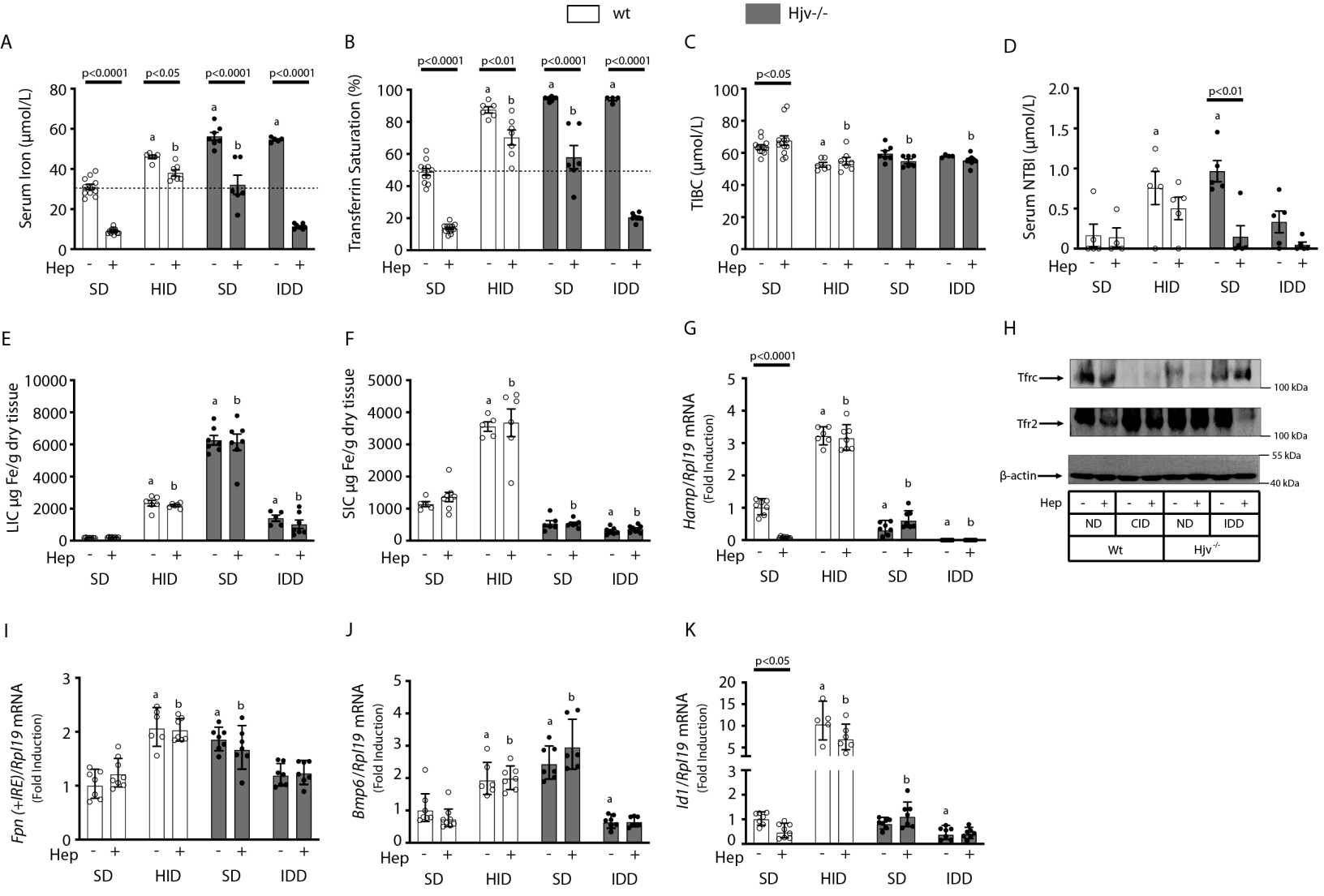

Fig. 4

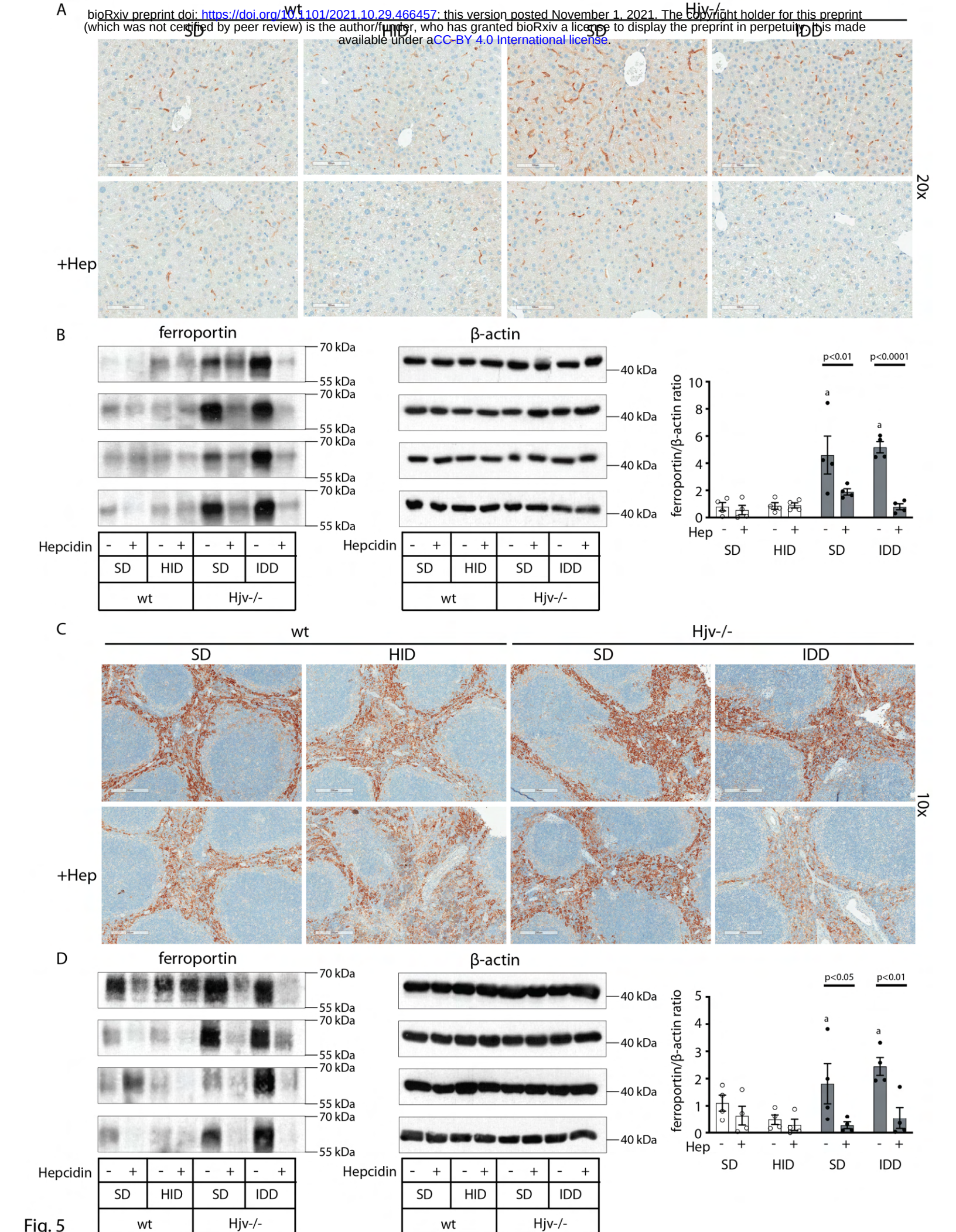

Fig. 5

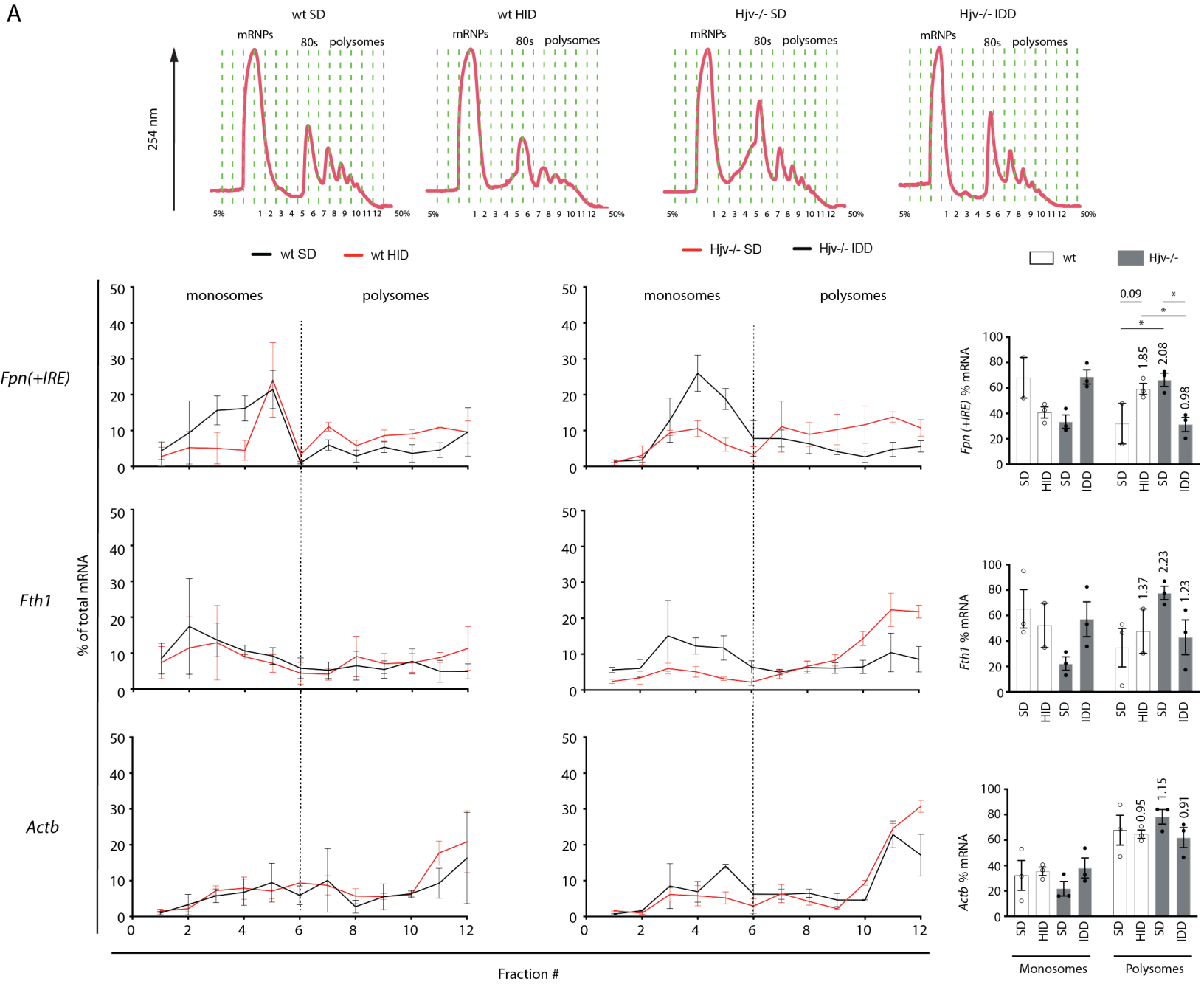

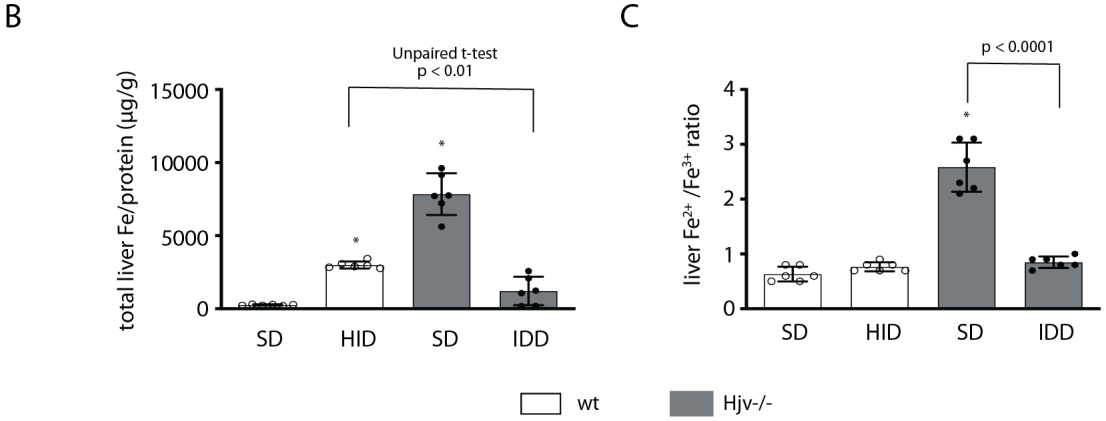

Fig. 6

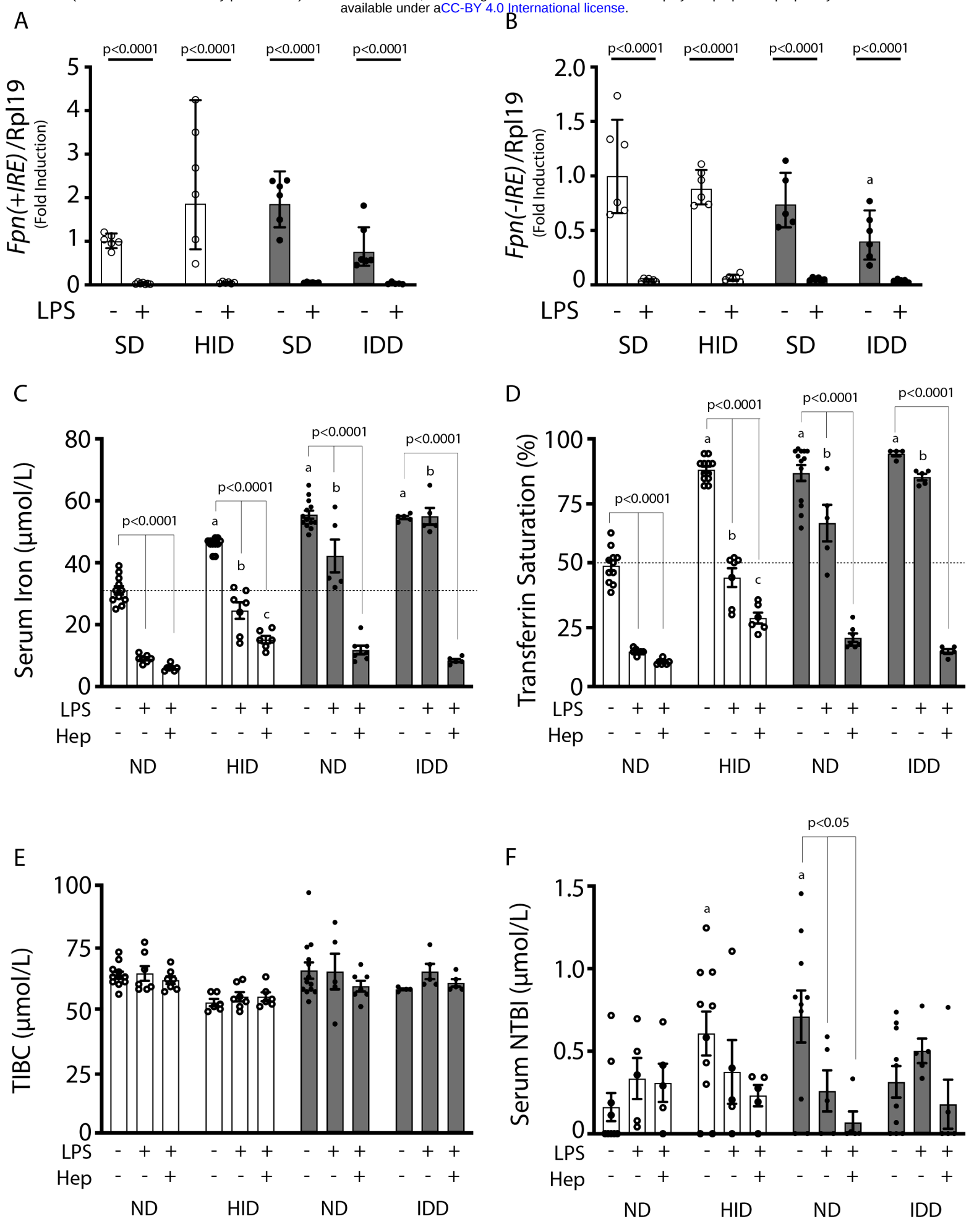

Fig. 7

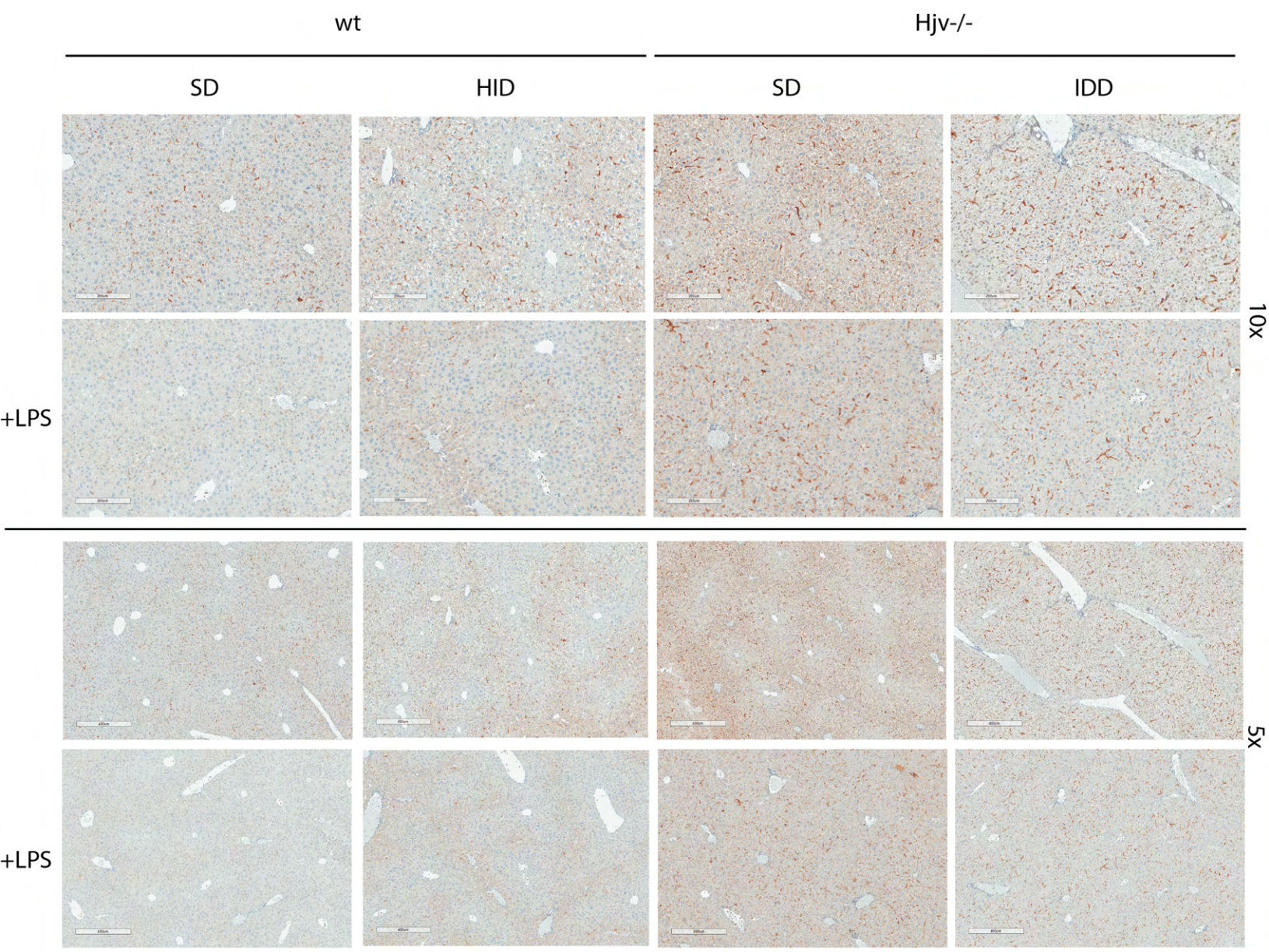

Fig. S1

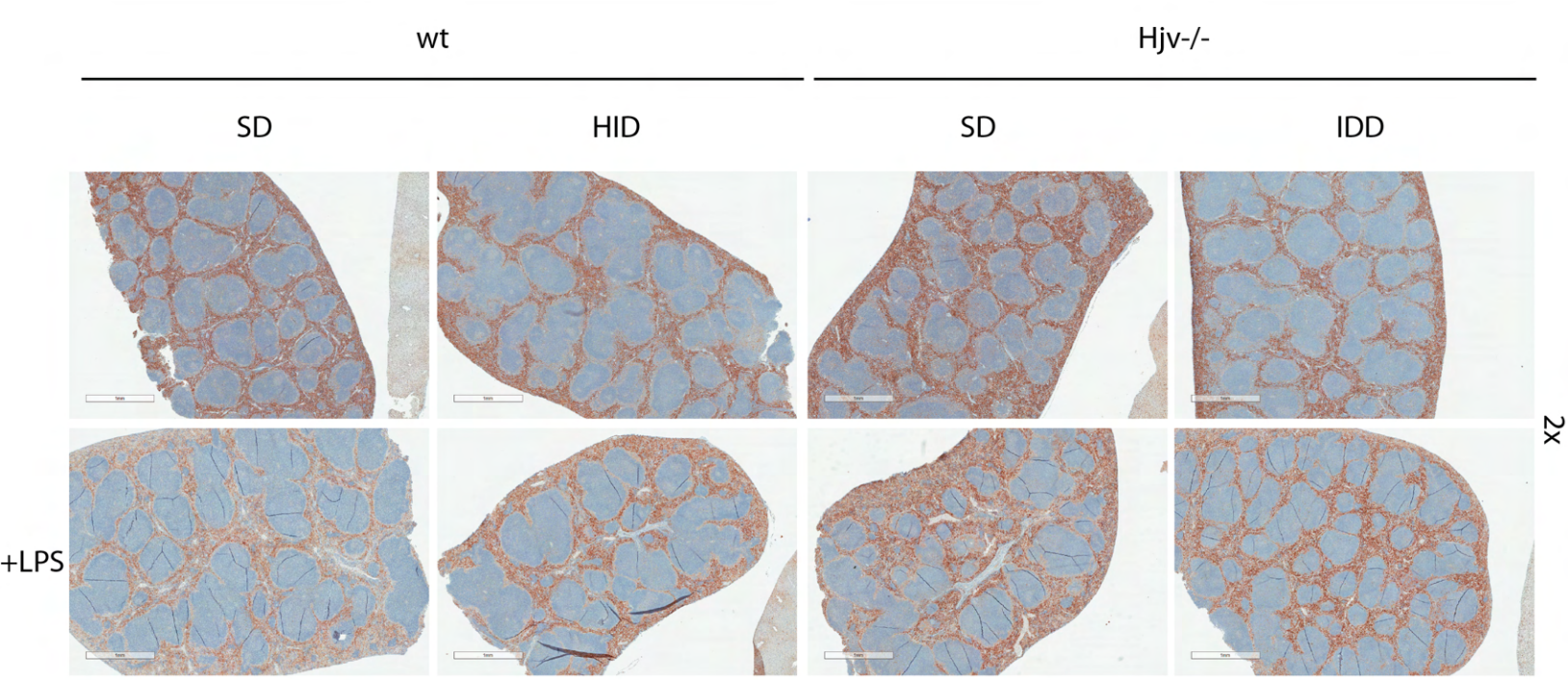

Fig. S2

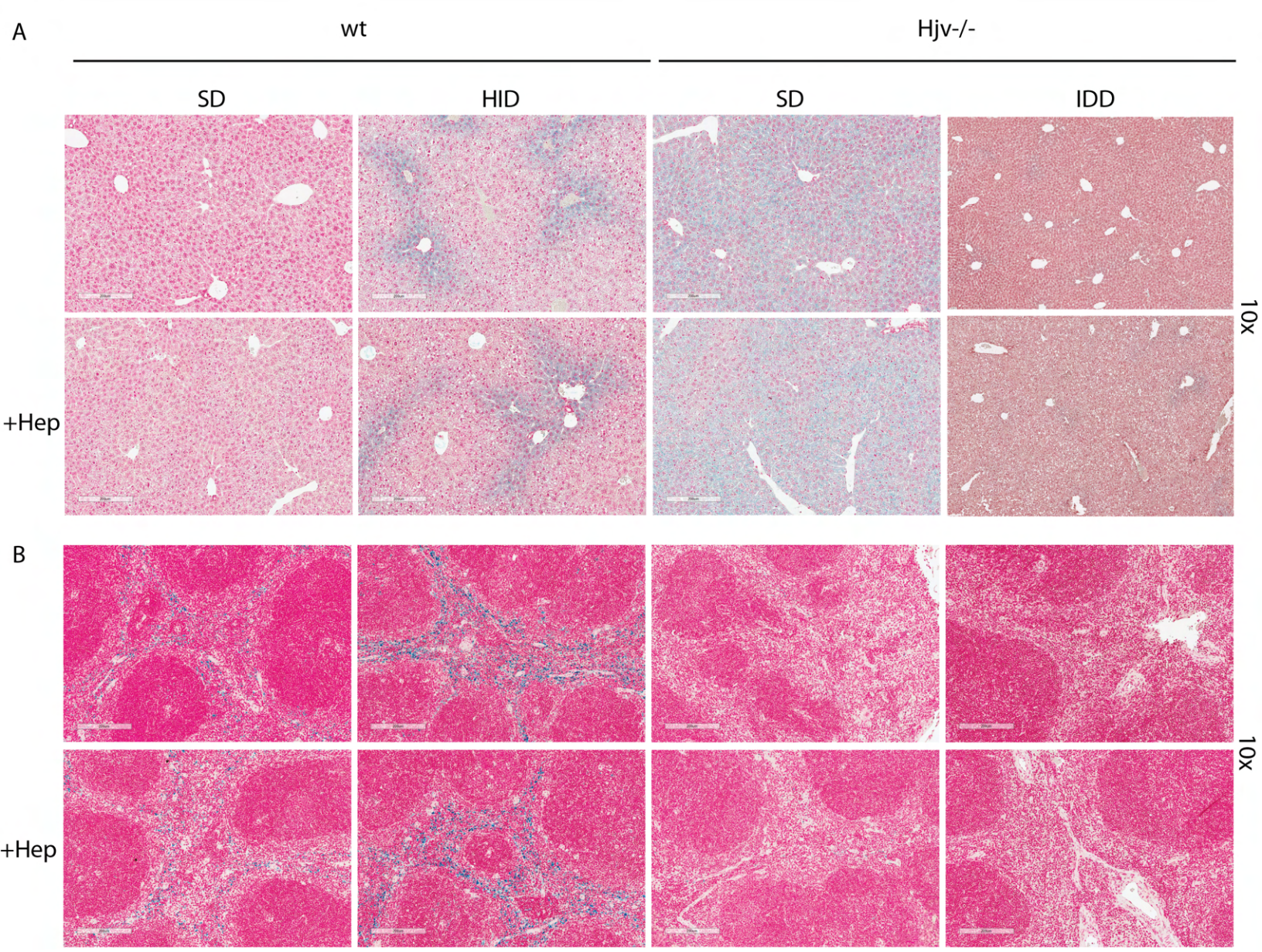

Fig. S3

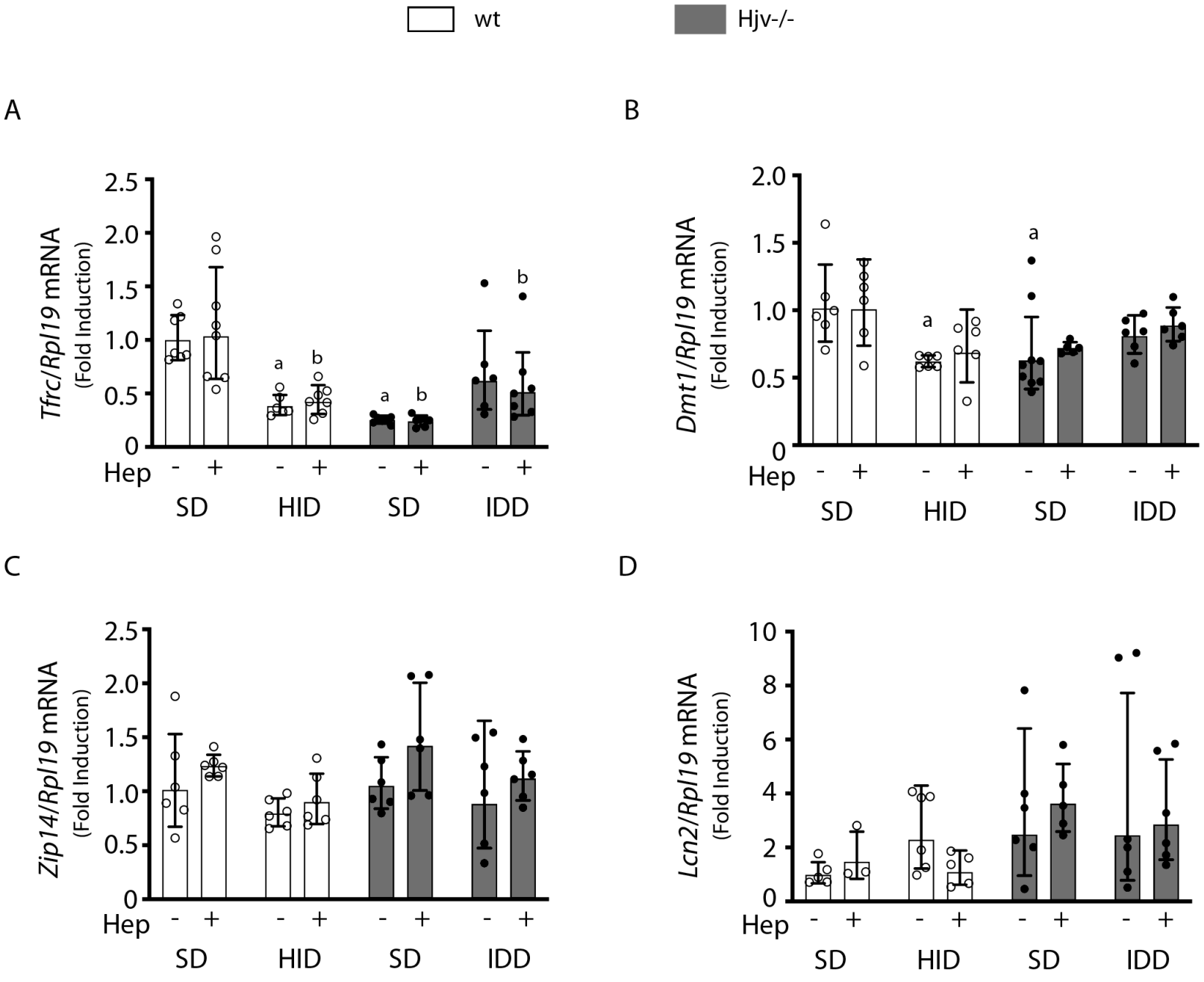

Fig. S4

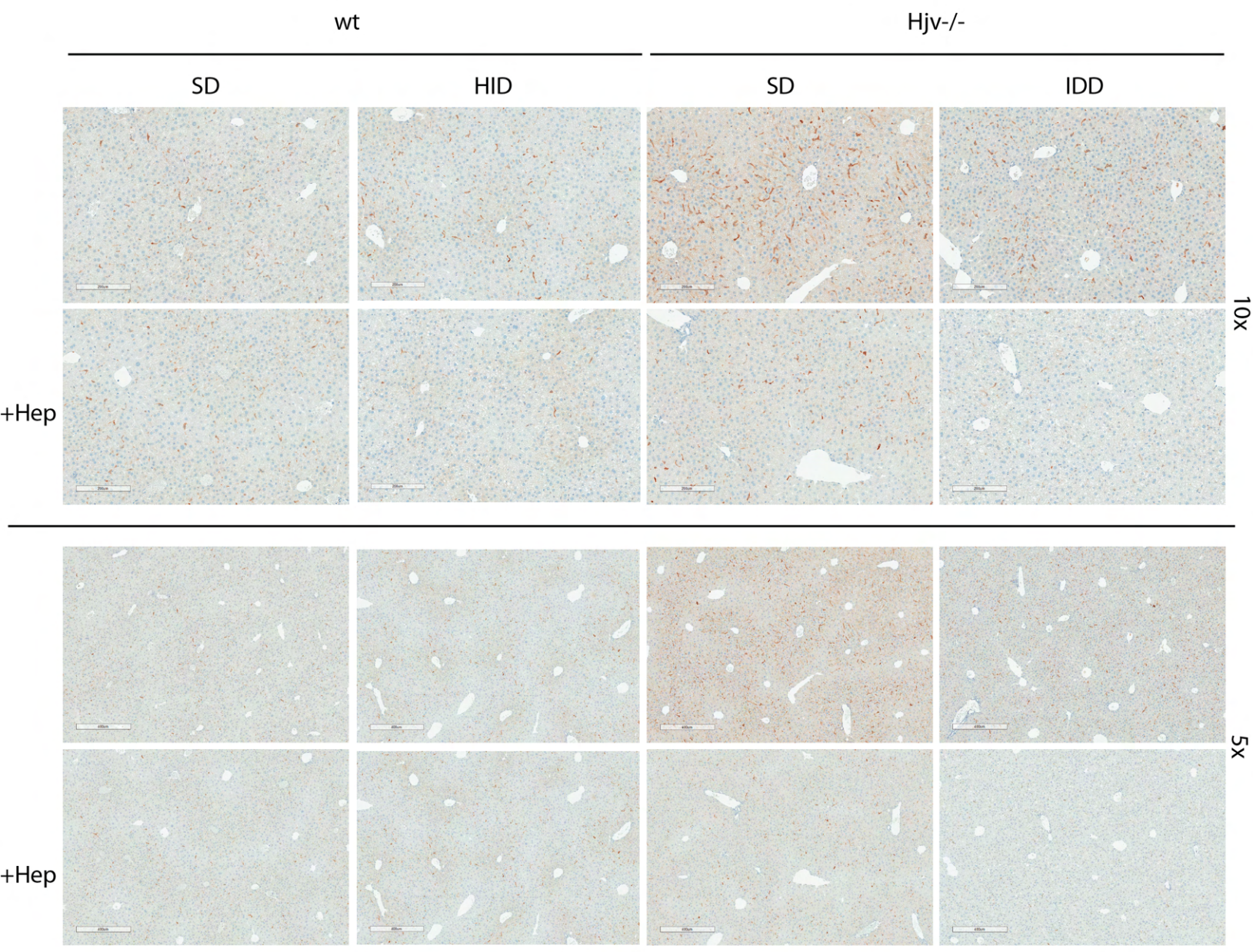

Fig. S5

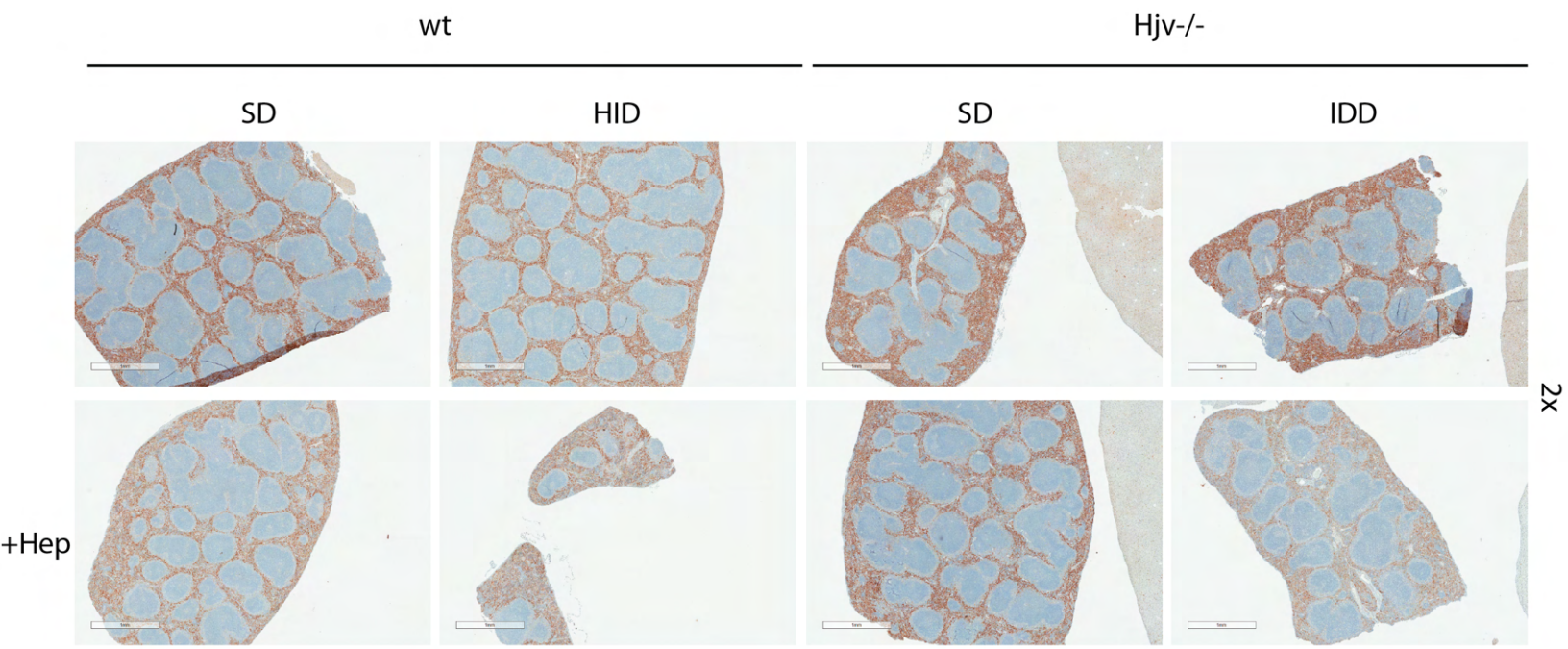

Fig. S6